THE ASTRONOMICAL JOURNAL, 118:162–185, 1999 July

A 180 KILOPARSEC TIDAL TAIL IN THE LUMINOUS INFRARED MERGER ARP 299

J. E. HIBBARD
National Radio Astronomy Observatory,[1] 520 Edgemont Road, Charlottesville, VA 22903; jhibbard@nrao.edu

AND

M. S. YUN
National Radio Astronomy Observatory,[1] P.O. Box O, Socorro, NM 87801; myun@nrao.edu
Received 1999 January 29; accepted 1999 March 15

ABSTRACT

We present VLA H I observations and University of Hawaii 88 inch (2.2 m) deep optical *B*- and *R*-band observations of the IR-luminous merger Arp 299 (=NGC 3690 + IC 694). These data reveal a gas-rich ($M_{\rm H\,I} = 3.3 \times 10^9\ M_\odot$) optically faint ($\mu_B \gtrsim 27$ mag arcsec^{-2}, $\mu_R \gtrsim 26$ mag arcsec^{-2}) tidal tail with a length of over 180 kpc. The size of this tidal feature necessitates an old interaction age for the merger ($\gtrsim$750 Myr since first periapse), which is currently experiencing a very young starburst ($\lesssim$20 Myr). The observations reveal a most remarkable structure within the tidal tail: it appears to be composed of two parallel filaments separated by approximately 20 kpc. One of the filaments is gas-rich with little if any starlight, while the other is gas-poor. We believe that this bifurcation results from a warped disk in one of the progenitors. The quantities and kinematics of the tidal H I suggest that Arp 299 results from the collision of a retrograde Sab–Sb galaxy (IC 694) and a prograde Sbc–Sc galaxy (NGC 3690) that occurred 750 Myr ago and will merge into a single object in roughly 60 Myr. We suggest that the present IR-luminous phase in this system is due in part to the retrograde spin of IC 694. Finally, we discuss the apparent lack of tidal dwarf galaxies within the tail.

Key words: galaxies: evolution — galaxies: individual (NGC 3690, IC 694, Arp 299) — galaxies: interactions — galaxies: ISM — galaxies: kinematics and dynamics — galaxies: peculiar — galaxies: starburst — infrared radiation

1. INTRODUCTION

Arp 299 is a nearby ($V_{\rm hel} = 3080$ km s^{-1})[2] peculiar system comprising two highly distorted disk galaxies, with NGC 3690 (=Mrk 171A = UGC 6471 = VV 118b) to the west and IC 694 (=Mrk 171B = UGC 6472 = VV 118a)[3] to the east. There is also a compact spheroidal galaxy lying approximately 1′ to the northwest, which is at the same velocity as Arp 299 (MCG +10-17-2a, $V_{\rm hel} = 3100$ km s^{-1}; Fairall 1971; Sargent 1972). Figure 1 presents a *B*-band image of this system, taken from the optical data described later in this paper. Each of the above named systems are labeled, as is the unrelated background bridge-tail-bar system, Arp 296.

Arp 299 appears to be in an advanced stage of merging, with the two disks in contact but the nuclei still separated by about 20″ (4.7 kpc).[4] This impression is supported by radio continuum and near-infrared (NIR) imaging (Gehrz, Sramek, & Weedman 1983) and millimeter spectral line observations (Casoli et al. 1989, 1999; Sargent & Scoville 1991; Aalto et al. 1997), which locate two major concentrations of molecular gas at peaks in the radio and NIR (regions A and B in Fig. 1, using the naming convention of Gehrz et al. 1983). Source A is identified with the nucleus of IC 694, while source B is identified with the nucleus of NGC 3690.[5] Another concentration of molecular gas occurs at the region of disk overlap (labeled C′-C in Fig. 1).

Spectroscopic observations of the NIR peaks in radio recombination lines (Anantharamaiah et al. 1993; Zhao et al. 1997), the mid-infrared (Dudley & Wynn-Williams 1993; Dudley 1998), the NIR (Gehrz et al. 1983; Beck, Turner, & Ho 1986; Nakagawa et al. 1989; Ridgeway, Wynn-Williams, & Becklin 1994; Doherty et al. 1995; Smith et al. 1996; Lançon, Rocca-Volmerang, & Thuan 1996), optical recombination lines (Bushouse & Gallagher 1984; Keel et al. 1985; Armus, Heckman, & Miley 1989), and in the UV (Augarde & Lequeux 1985; Kinney et al. 1993; Roberts 1996; Vacca et al. 1999) fail to reveal any definitive evidence for an AGN, and are consistent with the dominant energy source being a compact starburst (although there is evidence for some contribution from a compact source; see Shier, Rieke, & Rieke 1996; Carral, Turner, & Ho 1990; Jones, Gehrz, & Smith 1990; Jones 1997). This picture is consistent with continuum observations in the radio (Condon et al. 1982; Gehrz et al. 1983; Condon et al. 1990, 1991; Smith, Lonsdale, & Lonsdale 1998), far-infrared (Joy et al. 1989), NIR (Telesco, Decher, & Gatley 1985; Carico et al. 1990; Wynn-Williams et al. 1991; Miles et al. 1996), and X-ray (Rieke 1988; Zezas, Georgantopoulos, & Ward 1998).

Within the main body, vigorous star formation is taking place, with an inferred star formation rate (SFR) of about 50 $M_\odot$ yr^{-1} (Heckman, Armus, & Miley 1990) and an age of $\lesssim$20 Myr (Augarde & Lequeux 1985; Stanford 1989; Nakagawa et al. 1989; Meurer et al. 1995; Vacca et al. 1999). A deep Hα + [N II] image of this system reveals a "magnificent large-scale filamentary structure made up of

[1] The National Radio Astronomy Observatory is a facility of the National Science Foundation operated under cooperative agreement by Associated Universities, Inc.

[2] All radial velocities quoted in this paper are heliocentric.

[3] There is some confusion as to the naming of this system, which is addressed separately in the Appendix. In the following, we adopt the naming convention used most widely in the literature.

[4] Adopting the distance of 48 Mpc from Sanders, Scoville, & Soifer (1991), which assumes $H_0 = 75$ km s^{-1} Mpc^{-1} and the Virgocentric flow model of Aaronson et al. (1982). At this distance 1′ = 14 kpc.

[5] High-resolution NIR imaging by Wynn-Williams et al. (1991) shows that source B is itself a double, separated by about 3″.

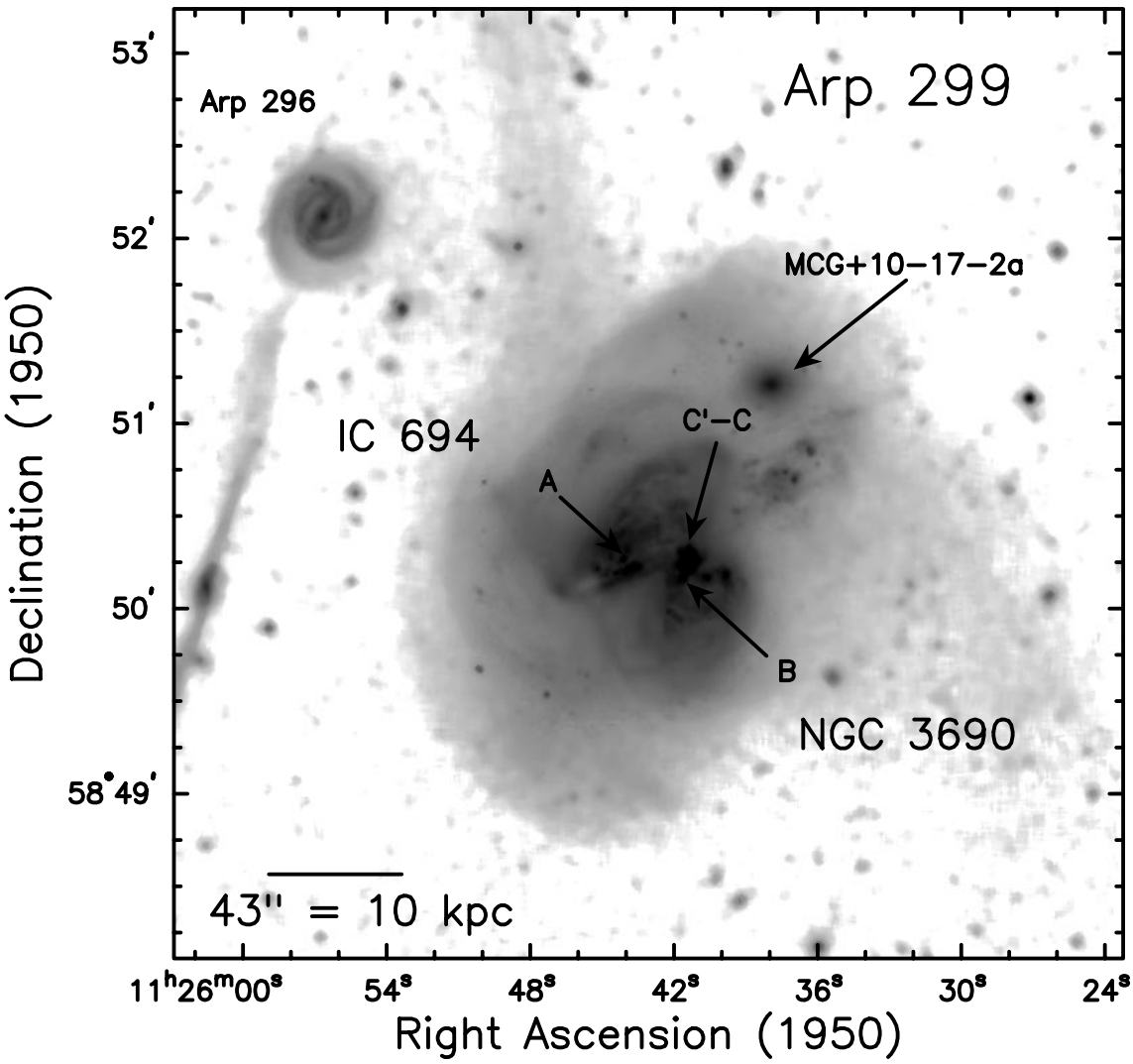

FIG. 1.—*B*-band image of the Arp 299 system. The optical image is displayed with a logarithmic transfer function, with white set to 28.5 mag arcsec^{-2} and black set to 22.75 mag arcsec^{-2}. IC 694 is to the left (east), NGC 3690 to the right, and north is up. Regions denoted "A," "B," and "C′-C" by Gehrz et al. (1983) are so labeled. We also identify the associated system MCG + 10-17-2a and the unrelated background bar-bridge-tail system Arp 296. A scale bar is drawn indicating 10 kpc, assuming a distance of 48 Mpc to Arp 299. The putative nuclei of the progenitors, as judged by NIR imaging and spectroscopy, are at regions A and B. Both of these locations are the sites of very dense molecular gas concentrations. The label "C′-C" indicates the region of disk overlap, which is also the site of a significant concentration of molecular gas.

arcs and loops that surround the galaxies at radii of about 6–12 kpc" (Armus, Heckman, & Miley 1990). Recent X-ray observations reported by Heckman et al. (1999) show evidence for hot gas emerging from the inner regions to the north, which the authors interpret as evidence for a hot, expanding superwind fluid.

The present Very Large Array (VLA) 21 cm observations of the neutral hydrogen (H I) in Arp 299 were conducted as part of a larger program to study the closest luminous IR galaxies in the IRAS Bright Galaxy Sample of Sanders, Scoville, & Soifer (1991). Arp 299 is both the most IR luminous member of this sample within a distance of 50 Mpc ($L_{IR} = 8.1 \times 10^{11}\ L_{\odot}$) and the closest system with an IR luminosity greater than $5 \times 10^{11}\ L_{\odot}$. It is therefore an important target to study for insight into the causes of such luminous starbursts. The purpose of the present study is to map any extended atomic hydrogen in order to constrain the encounter geometry and the Hubble types of the progenitors.

The paper is organized in the following manner. In § 2 we briefly describe the observations. In § 3 we present the observations separately for the inner regions, tidal regions, and for the H I absorption and a new H I detected companion. In § 4 we use the observations to explore the probable Hubble types of the progenitors, the encounter geometry, the possibility of self-gravitating entities within the tail, the conditions for an IR luminous phase, and the explanation for the differing H I and optical tidal morphologies. We summarize our main conclusions in § 5.

2. OBSERVATIONS

2.1. H I *Observations*

The VLA H I spectral-line observations were obtained as part of a study of the outer gas dynamics of IR luminous mergers (Hibbard & Yun 1996, 1999), and the data reduction techniques are fully described in that paper, except the continuum subtraction, which is described

below. The details of these observations are tabulated in Table 1. Briefly, the data consist of a 3.5 hr observation with the VLA in the C-array configuration (FWHM resolution $\theta_{\rm FWHM} \sim 15''$) and a 3 hr observation with the VLA in the D-array configuration ($\theta_{\rm FWHM} \sim 45''$). The data were combined in the UV plane to form the C + D configuration data that are used in the remainder of this paper. The correlator mode was chosen to provide 63 spectral channels with a channel spacing of 10.5 km s^{-1} and total bandwidth of 660 km s^{-1} centered at 3080 km s^{-1}. The data were reduced using standard reduction procedures in the Astronomical Image Processing System (AIPS).

The observations reveal broad H I absorption against the diskwide starburst and central radio continuum sources (see also Dickey 1982; Baan & Haschick 1990, hereafter BH90). This absorption was observed in channels 5–55 out of the 63 channel data cube (of which only channels 2–58 are useful). As a result, we could not achieve an optimal continuum subtraction by using line-free channels on either end of the bandpass, as is usually done (e.g., Rupen 1999). Instead, we mapped and "cleaned" the continuum image and subtracted the brightest 17 "clean components" from the UV line data, which accounts for approximately half of the total continuum flux of 820 mJy falling within the primary beam (FWHM = 30′). The line data were then mapped and cleaned in AIPS, resulting in a three-dimensional H I data "cube," with right ascension and declination along the first two coordinates and velocity along the third axis.

These data still contained many continuum sources, but were relatively free of the deep side lobes from the brighter sources. The residual continuum was removed in the map plane using a spatially variable continuum baseline. The H I tidal features appeared over a narrow range of velocity, and the residual continuum was removed from these regions by fitting a first order polynomial to a large number of channels on either side of this range. The emission from the northwest disk appears in channels 4–26, and the residual continuum was subtracted from this region by fitting to the continuum in channels 34–54. The emission from the southwest disk appears in channels 24–50, and the residual continuum was subtracted from this region by fitting to the continuum in channels 4–20. Finally, the residual continuum was removed from the regions showing H I absorption by fitting to the continuum in channels 2–4 and 52–58.

The data were mapped using different weighting functions to achieve varying resolutions and sensitivities. A high-resolution data cube was made using a "robust" parameter (R; Briggs 1995) of $R = 0$, which gives more weight to longer baselines and hence to smaller angular scales. This cube obtains a surface brightness sensitivity of 0.35 mJy beam^{-1} at a resolution of $\theta_{\rm FWHM} = 17'' \times 15''$. This corresponds to a column density limit (2.5 σ) of 4×10^{19} cm^{-2} averaged over the beam width of 4.0 × 3.4 kpc^2. A more sensitive intermediate-resolution data cube was made with $R = 1$, giving a resolution of $22'' \times 20''$ (5.1 × 4.7 kpc^2) and a column density limit of 2×10^{19} cm^{-2}. To further increase sensitivity to extended low column density gas, a low-resolution data cube was made by convolving the $R = 1$ data cube to a resolution of 35″ (8.1 kpc), reaching a detection limit of 1×10^{19} cm^{-2}. These data will be referred to in the following as the high-, intermediate-, and low-resolution data, respectively.

2.2. *Optical Observations*

The VLA observations reveal a gaseous stream of material extending to a radius of 9′ that had no known optical counterpart on existing images. As such, this region was targeted for deeper optical observations with the University of Hawaii 88″ telescope at Mauna Kea Observatory. The observational parameters are listed in Table 2. The Tek 2048 CCD was used with the f/10 reimaging optics, giving a plate scale of 0.″22 pixel^{-1} and a field of view of 7.′5. Three overlapping 600 s R-band images of the region of interest were obtained in 1995 January. In 1997 January we obtained a 600 s B-band image centered on the main body and two overlapping 900 s B-band images of the H I tail. The total imaged region covers an area of 8.′7 × 12.′4. The conditions were photometric on both dates, and the seeing was approximately 1″. The data were calibrated via observations of Landolt $UBVRI$ standards (Landolt 1983) observed on the same nights, with zero point errors (1 σ) of 0.01 mag in B and 0.03 mag in R.

TABLE 1

VLA Observing Parameters

Parameter		Value	
Phase center (α_{1950}, δ_{1950})	11 25 44.2	+58 50 18	
Velocity center (heliocentric; km s^{-1})		3080	
Primary beam (FWHM; arcmin)		30	
Phase calibrator		1203 + 645	
Flux calibrator		3C 268	
Bandwidth (MHz)		3.125	
Number of channels		63	
Channel separation (km s^{-1})		10.5	
Data set	D Array	C Array	C + D Array
Date	1995 Apr 18	1994 Dec 10	...
Synthesized beam:			
FWHM: Major axis × minor axis (arcsec)	56 × 46	17 × 15	22 × 20
Position angle (east of north; deg)	+37	−22	−12
Time on source (hr)	2.1	2.9	5.0
Noise level (1 σ):			
Flux density (mJy beam^{-1})	0.56	0.37	0.30
Column density ($\times 10^{19}$cm^{-2} beam^{-1} channel^{-1})	0.25	1.7	0.80
Brightness temperature (K beam^{-1})	0.13	0.88	0.41

TABLE 2

OPTICAL OBSERVING PARAMETERS

Parameter	Value	
Telescope (arcsec)	UH 88	
Detector	Tek 2048	
Readout Mode	Binned 1 × 1	
Focal Ratio	f/10	
Pixel Size (arcsec)	0.22	
Field of View:		
Single CCD Frame (arcmin)	7.5 × 7.5	
Final Image (arcmin)	8.7 × 12.4	
Filter	*R* Band	*B* Band
Date	1996 Jun 3	1996 Jan 7
Effective exposure time (s)	~2 × 600	~2 × 900
Seeing (arcsec)	1.2	0.9
Sky brightness (mag arcsec^{-2})	20.9	22.9
1 σ sky noise[a] (mag arcsec^{-2})	25.8	27.0
3 σ sky noise[b] (mag arcsec^{-2})	26.9	28.0

NOTE.—Units of right ascension are hours, minutes, and seconds, and units of declination are degrees, arcminutes, and arcseconds.

[a] 1 σ noise in original unbinned image.

[b] 3 σ noise after binning 9 × 9. This should be close to the 3σ detection limit, and we can often trace extended features to 0.5 mag fainter than this.

The images were flattened and combined using the techniques described in Hibbard & van Gorkom (1996, hereafter HvG96), and the final mosaics are flat to better than one part in 500. The combined image was transformed to the World Coordinate System (and thereby to the same reference frame as the radio images) by registering to an image of the same area extracted from Version II of the Digitized Sky Survey (XDSS),[6] obtained from the CD jukebox at the Canadian Astronomy Data Centre.[7] The registration was accomplished by referencing the location of about 20 stars in common on both images using the KOORDS program in the Karma software package (Gooch 1995) to perform a nonlinear least-squares fit for the transformation equations. The plate solution so found is better than a fraction of a pixel (0.″22), and the overall registration should be as good as that of the northern portion of the Guide Star Catalog, which is estimated to be 0.″5 (Taff et al. 1990).

Finally, a deep optical image was constructed by binning the pixels with the lowest light levels 9 × 9 to achieve a limiting surface brightness of $\mu_B = 28.2$ mag arcsec^{-2} and $\mu_R = 27.1$ mag arcsec^{-2} (2.5 σ; Table 2).

3. RESULTS

The luminosity for the main galaxies was calculated out to the $\mu_B = 26$ mag arcsec^{-2} isophote, and the corresponding *B* magnitude for the Arp 299 system ($m_B = 12.31$) agrees within 0.01 mag to that given by Mazzarella & Boroson (1993). These and other global parameters for the Arp 299 system are given in Table 3, and the entries are described in the notes to that table. In the following, we will discuss the

[6] The Second Palomar Observatory Sky Survey was made by the California Institute of Technology with funds from the National Science Foundation, the National Geographic Society, the Sloan Foundation, the Samuel Oschin Foundation, and the Eastman Kodak Corporation. The Oschin Schmidt Telescope is operated by the California Institute of Technology and Palomar Observatory.

[7] The Canadian Astronomy Data Center is operated by the Dominion Astrophysical Observatory for the National Research Council of Canada's Herzberg Institute of Astrophysics.

TABLE 3

MEASURED PROPERTIES OF THE ARP 299 SYSTEM

Quantity	Units	Total	Disk[a]	Tail	Companion[b]
Optical:					
L_B[c]	$L_{\odot,B}$	4.5×10^{10}	4.3×10^{10}	1.6×10^{9}	2×10^{9}
L_R[c]	$L_{\odot,R}$	4.9×10^{10}	4.7×10^{10}	1.2×10^{9}	2×10^{9}
B	mag	12.31			18
R	mag	11.04			17
H I (measured):					
Velocity range[d]	km s^{-1}	2800–3380	2910–3350	3020–3210	3230–3250
$\int S\,dv$	Jy km s^{-1}	17.7	11.7	6.1	0.14
$M_{\rm H\,I}$[e]	$M_\odot$	9.6×10^{9}	6.3×10^{9}	3.3×10^{9}	8×10^{7}
$M_{\rm H\,I}/L_B$	$M_\odot\,L_\odot^{-1}$	0.2	0.15	1.6	0.04
$M_{\rm H\,I}/L_R$	$M_\odot\,L_\odot^{-1}$	0.2	0.13	1.7	0.04
H I (corrected[f]):					
$\int S\,dv$	Jy km s^{-1}	21.7	15.7		
$M_{\rm H\,I}$	$M_\odot$	1.18×10^{10}	8.5×10^{9}		
$M_{\rm H\,I}/L_B$	$M_\odot\,L_\odot^{-1}$	0.3	0.20		
$M_{\rm H\,I}/L_R$	$M_\odot\,L_\odot^{-1}$	0.3	0.18		

[a] Disk values include contribution from minor-axis clump and western plume.

[b] H I detected companion located at $\alpha_{1950} = 11^{\rm h}24^{\rm m}28^{\rm s}.0$, $\delta_{1950} = +58°48'05''$ and $v_{\rm hel} = 3245$ km s^{-1}.

[c] Luminosities calculated assuming $M_{\odot,B} = +5.48$ and $M_{\odot,R} = +4.31$. Values for disk are measured to $\mu_B = 26$ mag arcsec^{-2}, $\mu_R = 25.5$ mag arcsec^{-2}. Values for tail are measured after removing point sources. The values for the companion are estimated from the DSS image and are very approximate (see text).

[d] Range of H I velocities (heliocentric). Taken from the first-moment image except for the total, which is the range seen in absorption. The uncertainty is ± 5 km s^{-1}.

[e] Integrated H I mass, calculated using $M_{\rm H\,I} = 2.356 \times 10^5 M_\odot\,\Delta^2 \int S\,dv$, where Δ is the distance in Mpc and $\int S\,dv$ is the integrated H I emissivity in Jy km s^{-1}. Following Sanders et al. (1991), we adopt 48 Mpc as the distance to Arp 299.

[f] Absorption corrected value (see text).

kinematics and morphology of the inner disk first and then that of the outer tidal features. We also discuss the central H I absorption and report the discovery of a small dwarf companion to Arp 299.

3.1. *Inner Gas Disk*

The disk H I kinematics are illustrated in Figures 2 and 3. Figure 2 presents several two-dimensional representations of the high-resolution H I data, with the emission summed over the third dimension. The upper left panel shows the integrated intensity map in solid contours (lowest contour corresponds to $N_{\rm H\,I} \sim 5 \times 10^{19}$ cm^{-2}) upon the *B*-band image. This map emphasizes higher column density material at the expense of the diffuse lower column density H I. We have therefore provided a dotted contour to indicate the $N_{\rm H\,I} = 2 \times 10^{19}$ cm^{-2} contour of the intermediate-resolution data, in order to give a more complete picture of the H I distribution in the inner regions. We have also labeled a minor-axis clump of H I and a western plume for reference in the following discussion.

To the right and below this panel are position-velocity maps constructed by summing the emission over declination (*lower panel*) or right ascension (*right panel*). Figure 3 presents the high-resolution channel maps of the inner disk alone, after Hanning-smoothing by a factor of 2 in velocity. In both of these maps, absorption is indicated by white dashed contours.

The inner H I disk was previously mapped with the VLA in the C-array configuration by Stanford & Wood (1989). As discussed by these authors, the kinematic signature seen in Figures 2 and 3 is representative of a rotating disk, with the northwest half of the disk receding and the southwest

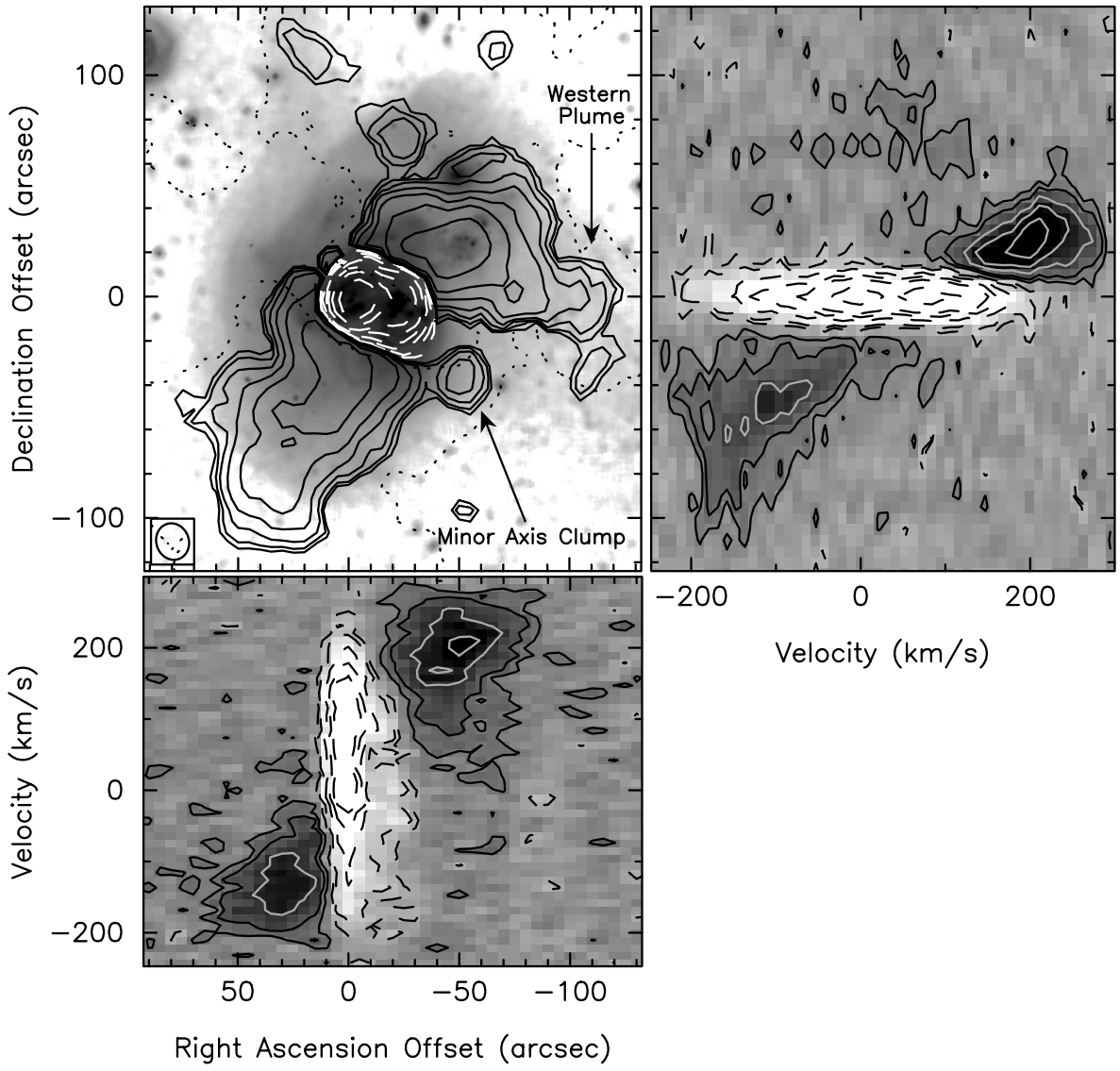

FIG. 2.—Position-velocity profiles of the inner regions of Arp 299, demonstrating the kinematics of the inner H I features. The top left panel presents the *B*-band image displayed in Fig. 1, with contours from the high-resolution H I integrated intensity map superposed (FWHM = 17″ × 15″, as indicated by the ellipse in the lower left corner of the panel). Negative contours are drawn as dotted white lines, indicating the region of H I absorption. The positive contours begin at 11.05 mJy beam^{-1} km s^{-1} (5×10^{19} cm^{-2}), while negative contours begin at −33.15 mJy beam^{-1} km s^{-1}. Successive contour levels are twice the previous level. The black dotted contour indicates a column density of 1×10^{19} cm^{-2} from the low-resolution H I data ($\theta_{\rm FWHM} = 35''$). To the right is a position-velocity map of the high-resolution data after summing the emission in right ascension, and below is a similar plot made by summing the emission in declination. Positions are measured relative to the nucleus of IC 694, and velocities are measured relative to 3100 km s^{-1}.

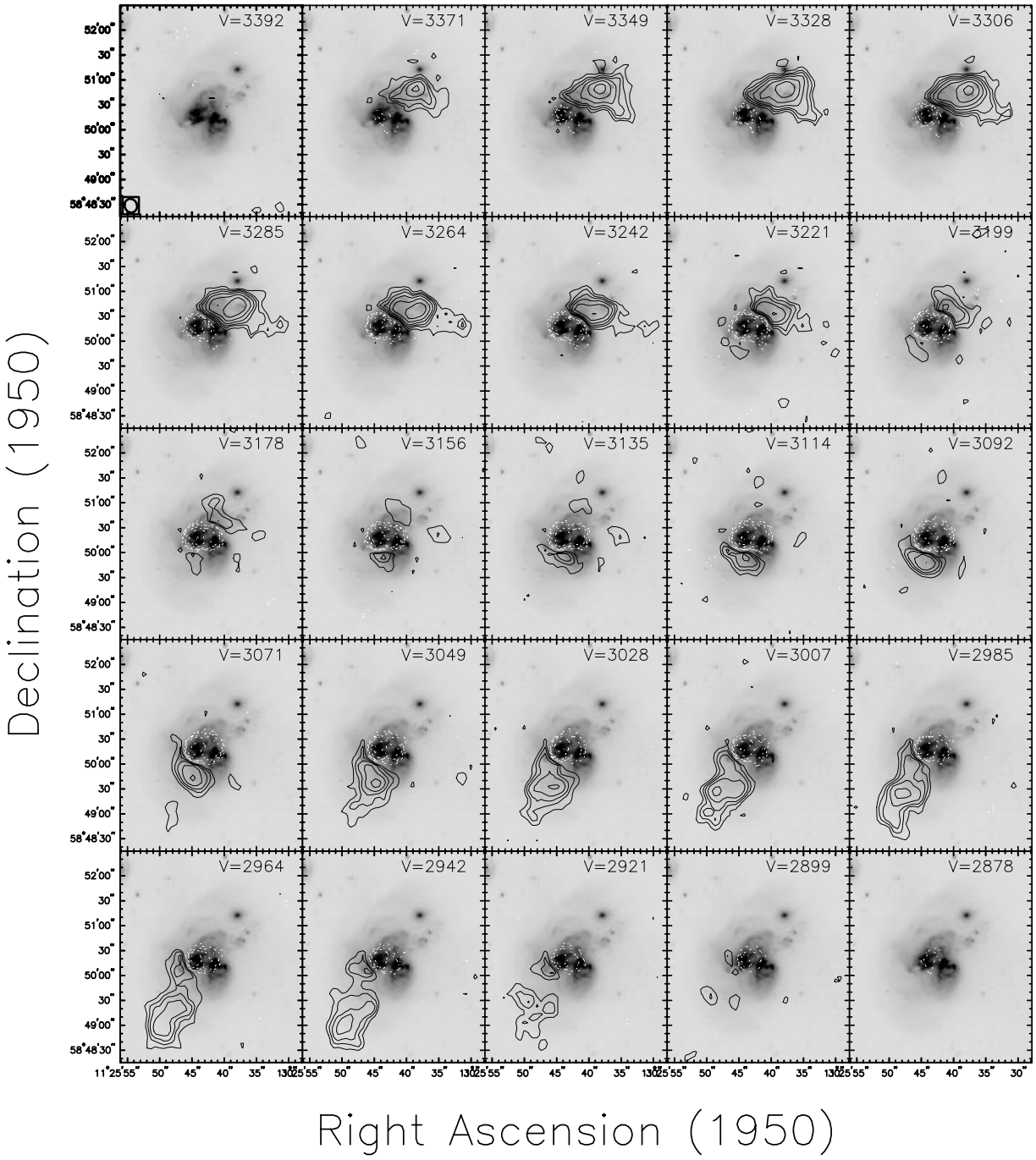

FIG. 3.—H I channel maps of the inner regions of Arp 299 contoured on the *B*-band image. The higher resolution data are used after Hanning smoothing in velocity by a factor of 2 to a channel spacing of 21.4 km s^{-1}. The beam size (17″ × 15″) is indicated in the lower left corner of the first panel, and each panel is labeled with the channel number and heliocentric velocity. Dotted white lines indicate negative contours, which are drawn at 1 σ × (−3, −5, −7, −10), where 1 σ = 0.25 mJy $beam^{-1}$ is the single channel noise level. Positive contours are drawn at 1 σ × (3, 5, 7, 10), with higher contours drawn a factor of 1.5 times the previous level. The lowest contour corresponds to a column density of 7.2×10^{19} cm^{-2}.

half approaching. The northwest component of the disk reaches a radius of 25 kpc and contains 2.9×10^9 $M_\odot$ of H I. The southeast component of the H I disk reaches a radius of 21 kpc and contains a total of 2.8×10^9 $M_\odot$ of atomic hydrogen.[8] The disk spans the velocity range from 2880–3390 km s^{-1}, with its kinematic center at 3135 km s^{-1}.

This disk was also mapped by the VLA in the D configuration by Nordgren et al. (1997) using a coarser velocity resolution (by a factor of 4) and a larger bandpass (by a factor of 2) than the observations presented here. Their observations suggest that the emission from the northwest disk continues to 3550 km s^{-1} (see their Fig. 7*b*), and therefore it is likely that we have missed some disk emission

[8] These masses do not include the contributions due to gas in the western plume or minor-axis clump discussed later.

because of our smaller velocity coverage. The OH maser emission from Arp 299 (Baan 1985; BH90) suggests that there may be nuclear gas at velocities as high as 3650 km s^{-1}.

The H I disk appears to be physically associated with the optically distorted disk of IC 694. This view is strongly supported by both the CO and Hα kinematics mapped at higher spatial resolution, as will be discussed in § 4.1 below. There are, however, emission features that deviate from this simple disk motion. There are $4.6 \times 10^8\ M_\odot$ of gas in a western extension to the northwest portion of the disk that appears to be kinematically associated with that disk (i.e., appears in the same velocity channels in Fig. 3) but which is spatially associated with a faint plume of starlight reaching to the southwest (labeled "western plume" in Fig. 2, see also Fig. 1). There are also $1.5 \times 10^8\ M_\odot$ of gas in a clump lying along the southwest minor axis of the disk (labeled "minor axis clump" in Fig. 2). If this minor-axis material were associated with the disk of IC 694, it would appear in only a few spectral channels. Since it appears over a broad range of velocities (from 3050–3200 km s^{-1} in Fig. 3), we suggest instead that it is associated with NGC 3690 (see § 4.1). There is also some emission associated with the base of the tidal tail (seen in the right panel of Fig. 2 toward the north and in the channel maps from 3092–3135 km s^{-1}), which is seen more clearly in the low-resolution maps discussed in the next section. Finally, there are some H I features that project close to the compact spheroidal galaxy MCG +10-17-2a (Fig. 3, channels at 3306–3371 km s^{-1}). Since these features appear at velocities that are higher than the velocity of MCG +10-17-2a itself ($V_{\rm hel} = 3100$ km s^{-1}; Fairall 1971; Sargent 1972) and close to the velocities of the H I within the underlying disk of IC 694, it seems likely that they are due to disk material that was perturbed by a recent close passage of the spheroidal.

3.2. *Outer Tidal Morphology*

Our VLA observations revealed a previously unknown tidal tail reaching 124 kpc in radius to the north. This discovery was initially reported in Hibbard & Yun (1996). Subsequently, VLA D-array observations of Arp 299 from 1995 May were published by Nordgren et al. (1997), confirming both the H I and optical tidal tail we report on in this paper.

In Figure 4 we show the H I integrated intensity map from the intermediate-resolution data, with position-velocity profiles plotted along either axis as in Figure 2. The tail appears as two parallel filaments separated by about 20 kpc (labeled "inner filament" and "outer filament" in Fig. 4), extending northward and connecting onto or merging into a dense clump of gas (labeled "N Clump" in Fig. 4). The inner filament originates near the minor axis of IC 694 (see also the northernmost clump in Fig. 2), appears broken at the lowest contour drawn in Figure 4 ($N_{\rm H\,I} \sim 2.5 \times 10^{19}$ cm^{-2}) after which there appears an H I density peak ($N_{\rm H\,I,peak} \sim 2 \times 10^{20}$ cm^{-2}, labeled "H I knot" in Fig. 4), and the filament continues northward. This inner filament contains a total of $4.4 \times 10^8\ M_\odot$ of neutral atomic hydrogen. The outer filament originates to the west of the first (see also the second northernmost clump in Fig. 2), is more complete and of a higher average column density than the inner filament ($N_{\rm H\,I} \sim 1 \times 10^{20}$ cm^{-2}), and contains twice as much H I ($M_{\rm H\,I} = 9 \times 10^8\ M_\odot$). The filaments join at the N clump, which contains $2 \times 10^9\ M_\odot$ of H I. This clump has an irregular column density distribution with peaks as high as 3×10^{20} cm^{-2}. The kinematics of these features will be discussed in the next section.

The tail reaches a maximum projected radial separation of 8.′6 (124 kpc; measured from source A to the outer contour in Fig. 4), and it extends 12.′7 or 180 kpc as measured along its length (measured from source A along the peak H I column density contour of the outermost feature). It contains a total of $3.3 \times 10^9\ M_\odot$ of atomic hydrogen, which is at the upper end of the tidal gas content of other major disk-disk mergers (HvG96; Hibbard & Yun 1999). Since less than half of the progenitor disk material can be raised into a tail, and most of this falls back quickly onto the remnant (Hibbard & Mihos 1995), this amount of tidal H I requires a very H I-rich progenitor ($M_{\rm H\,I} \sim 10^{10}\ M_\odot$). This point will be explored in more detail in § 4.2.

The deep optical imaging reveals a faint stellar tail extending in the same direction as the H I features (see Figs. 5, 6, and 7). The optical tail appears to emerge in the north near the minor axis of the system and curve slightly to the northeast to a radius of 9′. The width of the optical tail appears remarkably constant at about 1′ (14 kpc), although there may be some widening in the *B*-band image. The observed width of the tail can be understood as the result of the dispersal of outer disk stars with a typical velocity dispersion of 20 km s^{-1} (e.g., van der Kruit 1988; Bottema 1993) over an interaction age of 750 Myr (§ 4.1). At very faint light levels the tail appears to loop south and west from the northeast tip toward the bright star labeled "Star 2" in Figure 5*a*, with perhaps a very faint extension directly south of this star. While scattered light from the stars labeled "1" and "2" in this figure make the precise morphology of the faint optical light uncertain, these features have the same morphology in both the *B*- and *R*-band gray-scale images of Figure 5, while the scattered light properties are different between the bands (see, e.g., the difference between the faint scattered light associated with star 3 in Figs. 5*a* and 5*b*), and we feel confident that the faint optical features are not artifacts.

Upon first examination the optical and H I tidal features appear similar. But when the data are overlaid, as in Figures 6 and 7*b*, the differences in the distribution are striking: the inner H I filament roughly aligns with the optical tail, while the outer parallel H I filament has no corresponding optical feature down to the faintest levels measured ($\mu_B \sim 28.5$ mag arcsec^{-2}, $\mu_R \sim 27.5$ mag arcsec^{-2}).

Even within the optical tail, there is a poor correlation between optical and gaseous density peaks. If anything, the gas peaks seem to be displaced a bit to the west of the optical peaks. Neither the gap nor the knot in the inner H I filament appear to coincide with any discrete optical feature, although the optical surface brightness drops by about 1 mag arcsec^{-2} just north of the knot (Fig. 5). The displacements are even more extreme in the northernmost regions of the tail, where the gas and starlight appear to be anticorrelated: to either side of the optical tail there are regions of high gas column density ($N_{\rm H\,I} \sim 3 \times 10^{20}$ cm^{-2} to the west, $N_{\rm H\,I} \sim 2 \times 10^{20}$ cm^{-2} to the east), whereas the gas within the tail has $N_{\rm H\,I} \sim 1 \times 10^{20}$ cm^{-2}. At its northernmost extent, the optical tail has no associated H I and actually appears to "hook" toward the east, *exactly* around the northern H I contours in Fig. 7*b*.

This anticorrelation suggests the possibility that dust associated with the H I gas is playing a role in shaping the

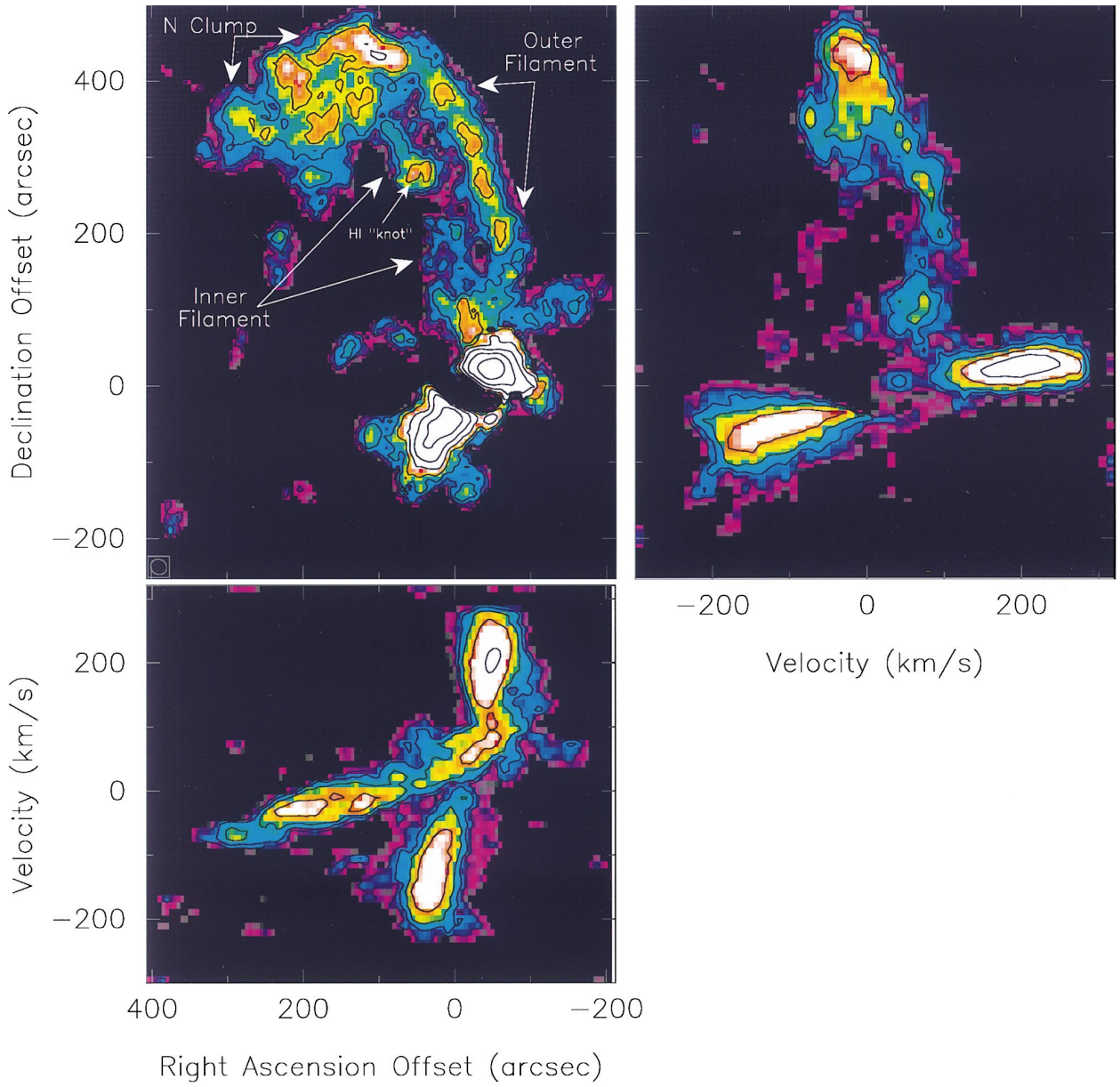

FIG. 4.—Position-velocity profiles of the entire Arp 299 system, demonstrating the kinematics of the tidal H I features. The top left panel presents a false-color and contoured image of the intermediate-resolution data cube (22″ × 20″). Features referred to in the text are labeled. The adjacent panels are position-velocity profiles, constructed by summing the data cube in right ascension (*right*) or declination (*bottom*). Values below 1 σ were not used when constructing the position-velocity plots. Contours are drawn starting at a level of 8 mJy beam^{-1} km s^{-1} (2×10^{19} cm^{-2}), with higher contours drawn a factor of 2 times the previous level.

optical tidal morphology. It is possible that extinction affects the optical morphology at the lowest light levels (e.g., at the northernmost "hook," $\mu_B \gtrsim 28$ mag arcsec^2). However, it is not likely to be hiding an optical counterpart to the outer filament, since the required amount of extinction (>1 mag at $N_{\rm H\,I} = 2 \times 10^{20}$ cm^{-2}) is an order of magnitude larger than measured for Galactic H I (Bohlin, Savage, & Drake 1978). Since tails are drawn from the outer, presumably dust-poor regions of disks, such a high gas-to-dust ratio seems unlikely (see also Alton et al. 1998). Evidence for just such a high gas-to-dust content in tidal gas may be indicated by observations of red globular clusters behind an H I tidal stream in NGC 5018 (Hilker & Kissler-Patig 1996). Still, we feel that this explanation is ruled out for Arp 299 by the fact that the optical tail is actually bluer north of the H I knot, where the H I column density is highest, compared with the starlight in the "gap" in the inner H I filament, where the H I column density is lowest (Fig. 7*a*). One would expect the opposite trend if there was a high gas-to-dust ratio in this tidal gas (see, however, Witt, Thronson, & Capuano 1992). The $B-R$ colors of the stellar tail range from 0.3–1.8, similar to range found in the outer stellar disk of late-type galaxies (de Jong 1995) and in other tailed mergers (Schombert, Wallin, & Struck-Marcell 1990; Hibbard et al. 1994; Hibbard 1995).

The total stellar content of the optical tail was estimated by masking the optical images below $\mu_B = 28$ mag arcsec^{-2} and $\mu_R = 27$ mag arcsec^{-2} and replacing regions containing point sources (presumably background sources; see § 4.5) and the optical halos of stars 1 and 2 in Figure 5*a* with

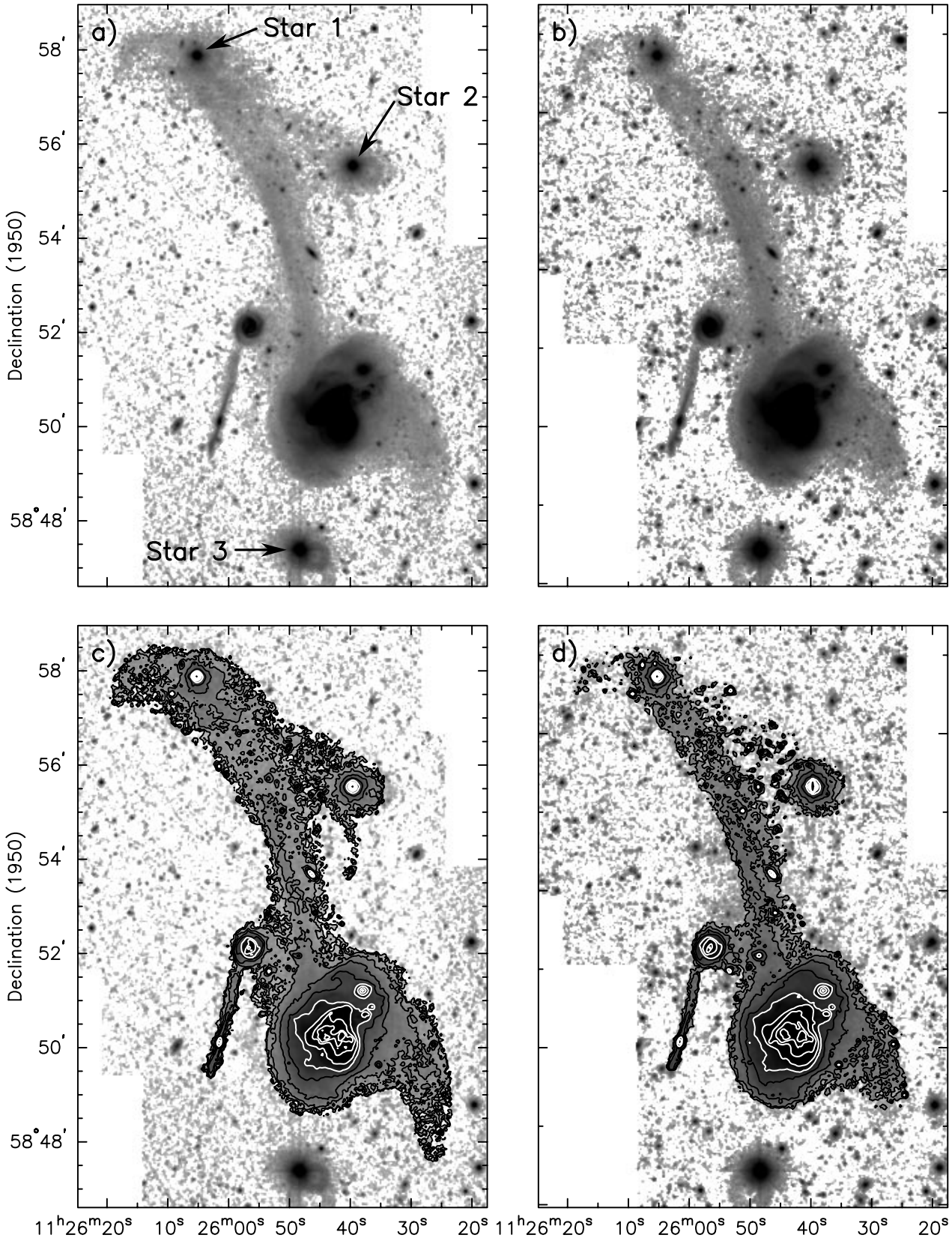

FIG. 5.—Deep optical image of the entire Arp 299 CCD mosaic, showing the total extent of the stellar tail. The deep *B*- and *R*-band data are shown on the left and right, respectively, using a logarithmic transfer function. Panels (*a*) and (*b*) show a gray-scaled representation of the data, while the panels (*c*) and (*d*) add contours. The gray scales give a better feeling for the structure at the lowest light levels, while the contoured images provide a quantitative measure of the light peaks. The gray scales cover the range $\mu_B = 28.5$ mag arcsec^{-2}–22.75 mag arcsec^{-2} and $\mu_R = 28.5$ mag arcsec^{-2}–22.0 mag arcsec^{-2}. In panels (*c*) and (*d*), white contours are drawn every 1 mag arcsec^{-2} starting at $\mu_B = 24$ mag arcsec^{-2} and $\mu_R = 25$ mag arcsec^{-2}, and black contours are added every 1 mag arcsec^{-2} starting at $\mu_B = 28$ mag arcsec^{-2} and $\mu_R = 27$ mag arcsec^{-2}. Three stars referred to in the text are labeled in panel (*a*).

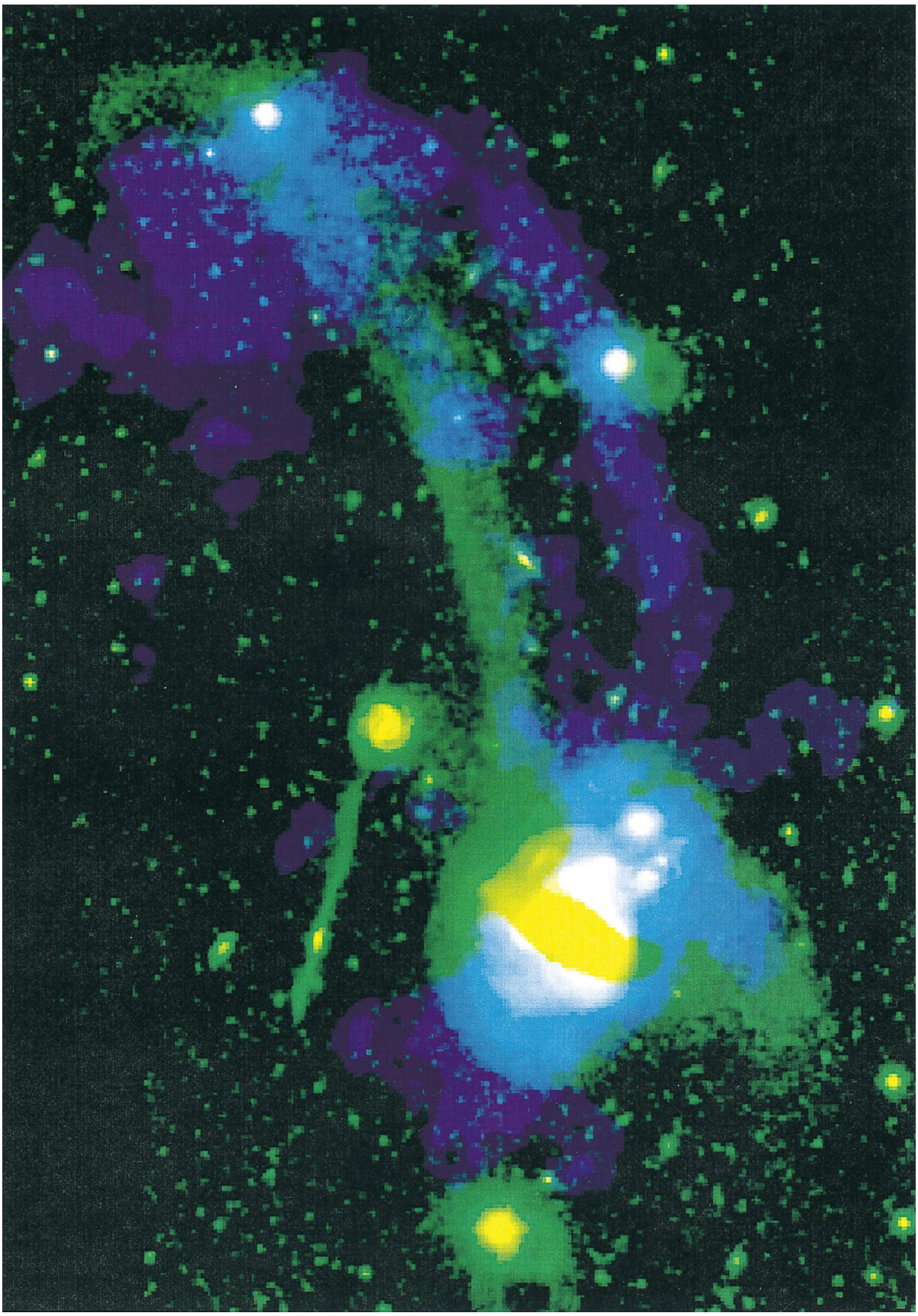

FIG. 6.—RGB representation of the Arp 299 optical and H I data. Yellow and green indicates optical emission, while blue indicates H I emission. Regions containing both forms of emission appear as the sum of these colors. This figure emphasizes the differences between the stellar and gaseous tidal morphologies.

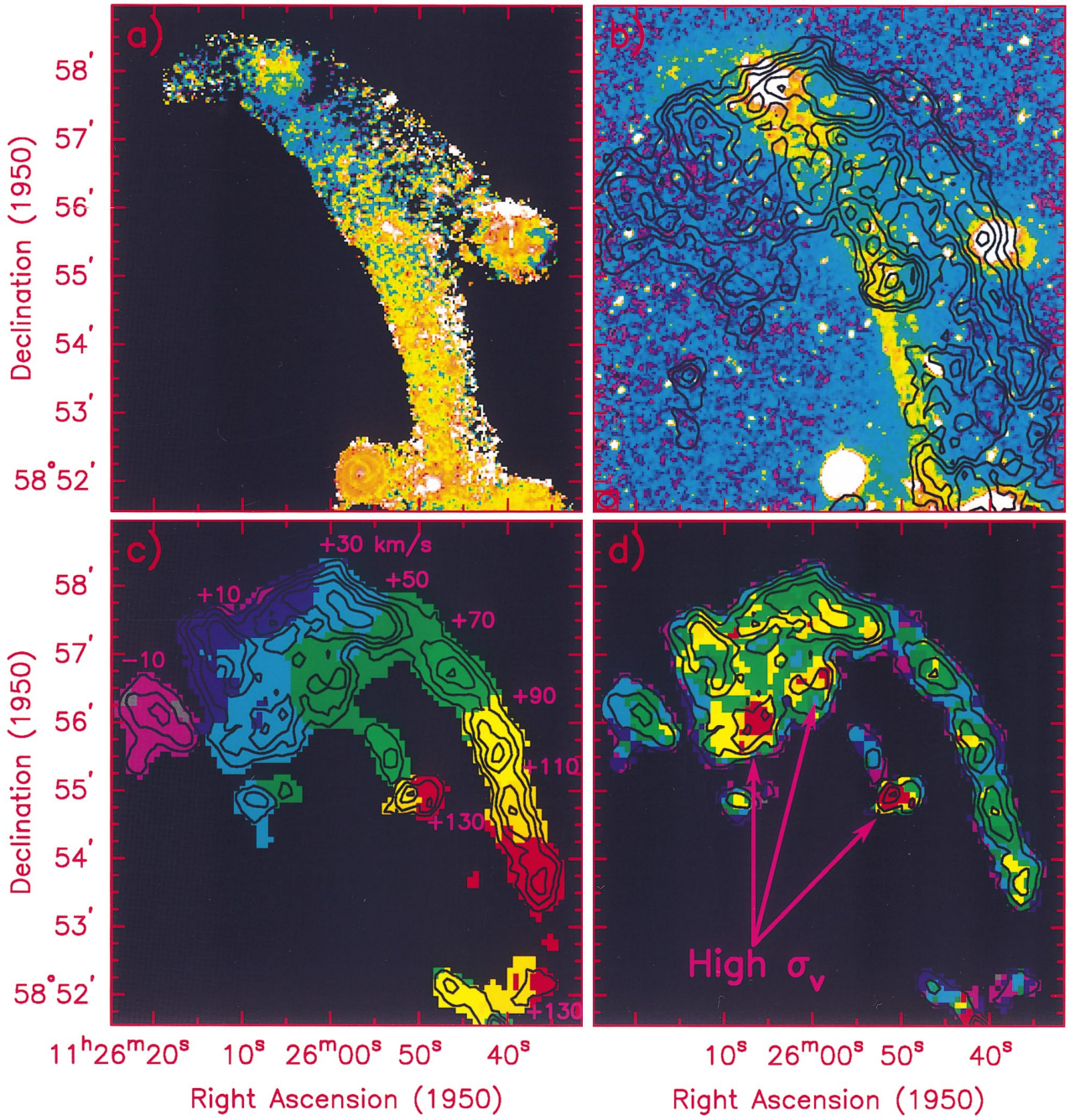

FIG. 7.—Detail of the Arp 299 tidal tail, showing the relationship between the gaseous and stellar morphologies and kinematics. (*a*) $B-R$ color map constructed from the smoothed data using only pixels with signal-to-noise ≥ 3 in both the *B*- and *R*-band images. A spectral transfer function is used with the following color mappings: Purple: $B-R < -0.2$ mag; blues: $B-R = -0.2-+1.0$; green-yellow: $B-R = 1.0$–2.0 mag; red: $B-R > 2.0$ mag. (*b*) False-color rendition of the *B*-band data with contours of the intermediate-resolution data overlaid. Contours are drawn at levels of 4 mJy km s^{-1} beam^{-1} (1×10^{19} cm^{-2}) $\times$ (3, 6 10, 15, 20, 25). (*c*) Intensity-weighted mean H I line-of-sight velocity. The intermediate-resolution data has again been used, but with a higher threshold for the moment algorithm. The color boundaries are indicated with labels giving the velocity (in km s^{-1}) with respect to NGC 3690 ($V_{\rm hel} \approx 3040$ km s^{-1}; see § 3.4). Contours are drawn at (1×10^{19}) $\times$ (5, 10, 15, 20, 30). (*d*) H I line-of-sight velocity dispersion, using the same data and threshold as in (*c*). The colors correspond to the following velocity dispersion ranges: purple-blue = 5–8 km s^{-1}; green = 8–10 km s^{-1}; yellow-orange = 10–13 km s^{-1}; red = 13–20 km s^{-1}. The regions of high-velocity dispersion discussed in § 3.3 and § 4.5 are indicated.

adjacent background values. The total optical light in the northern tail is $L_B = 1.6 \times 10^9$ $L_{\odot,B}$ and $L_R = 1.2 \times 10^9$ $L_{\odot,R}$, corresponding to 4% and 2% of the total *B*- and *R*-band light of the system, respectively[9] (Table 3). These percentages are on the lower end of the values found in peculiar systems (Schombert et al. 1990; Hibbard et al. 1994; HvG96).

The total H I mass-to-blue light ratios (in solar units) for all the northern tidal features is $M_{\rm H\,I}/L_B = 1.8$. There is quite a variation within the tail, with $M_{\rm H\,I}/L_B \sim 0$–1 along

the optical tail and ranging from 2 to over 10 for the outer filament and eastern regions of the N clump. The faint plume of light extending 45 kpc in radius to the west of Arp 299 contains $L_B = 1 \times 10^9\ L_{\odot,B}$. Associating the western H I extension to this feature gives $M_{\rm H\,I}/L_B = 0.5$.

3.3. *Outer Tidal Kinematics*

The kinematics of the tidal regions are illustrated by the integrated position-velocity profiles in Figure 4, intensity weighted velocities and velocity dispersions in Figures 7*c* and 7*d*, individual channel maps in Figure 8, and two- position velocity slices through either H I filament in Figure 9. Both Figures 8 and 9 are constructed from the low-resolution data cube, and the lowest plotted contour corresponds to a column density of 1×10^{19} cm^{-2}. The channel maps are only plotted over the velocity range containing tail emission.

The kinematics immediately illustrate two important points. The first is that the tidal kinematics are smooth, continuous, and single valued, as expected for tidal features (e.g., Barnes 1988; Hibbard et al. 1994; Hibbard & Mihos 1995). The second is that the two H I filaments share the same kinematics. This is best seen in Figure 8, in which the H I emission associated with parallel regions along the filaments appears in identical channels all along the tail. This rules out the possibility that the two filaments are separate tidal tails that are simply projected near each other; they must be different regions of the same kinematic structure. The figures also show that the N clump is continuous with the filaments and not a distinct entity. Therefore, the N clump and two filaments form a single contiguous feature in both space and velocity.

A more detailed comparison of the filament kinematics is shown in Figure 9, where we have plotted position-velocity profiles along both. This figure shows that the base of the outer filament has a slightly higher mean velocity than the base of the inner filament, which may help in deciding the relative morphologies, although we await detailed kinematic modeling before deciding how to interpret this information. Figure 9 illustrates a few more interesting properties of the filaments. In Figure 9*b* we see that the apparent "gap" in the integrated intensity map of Figure 4 is not devoid of H I: weak emission that did not pass the threshold used when making the moment maps bridges this gap (see also the panel at 3150 km s^{-1} in Fig. 8). We also see that the "knot" within the inner filament has an anomalously large velocity width (see also line-width map in Fig. 7*d*): the majority of the tail has a velocity dispersion of 7–9 km s^{-1}, which is typical of tidal tails in general (Hibbard et al. 1994; HvG96), while the knot has a dispersion of over twice this (20 km s^{-1}). Figure 7*d* shows that there are two additional velocity dispersion peaks along the southern edge of the N clump, with dispersions of 17 km s^{-1} and 13.5 km s^{-1} compared to an average dispersion of 10.5 km s^{-1} within the N clump. None of these regions corresponds to any noticeable features in the optical images or color maps, which argues against their being related to the putative tidal dwarf galaxies, a question we investigate in more detail in § 4.5.

Finally, there is a high velocity envelope of material just north of the knot (indicated in Fig. 9*b*). A similar envelope of material is seen at parallel locations in the outer filament (Fig. 9*d*). The channel maps show that this gas lies exactly along the faint optical light that stretches from the end of the tail toward star 2 in Figure 5*a* (see panels at 3171–3161 km s^{-1} in Fig. 8), while the majority of the filament gas has lower velocities and lies north of this light (see panels at 3098–3140 km s^{-1} in Fig. 8). These are probably important clues to the origin of these filaments, although we are at a loss to say what.

3.4. *Central Absorption*

High-resolution ($\sim 5''$) VLA radio continuum observations show that half of the total 1.4 GHz radio continuum emission lies within $5''$ of regions A, B, and C′-C in Figure 1, with the other half of the flux distributed between these regions and throughout the disk of IC 694 (Gehrz et al. 1983). Even higher resolution ($\theta_{\rm FWHM} = 1''.7$) VLA A-array observations of the H I absorption against these continuum sources are presented in BH90, along with observations of OH megamaser emission. These observations show that H I absorption is seen against all of the compact continuum sources as well as against the extended continuum features. Our continuum profiles are quite similar to those published by BH90, with subtle differences that are likely due to our larger beam, which allows surrounding H I emission to fill in some of the absorption. We will therefore use the results of the higher resolution H I absorption observations in concert with our H I emission observations to set some rough limits on the spin temperature ($T_{\rm spin}$) of the H I gas. Along the way, we will estimate the absorbing column of gas in front of the continuum sources, from which we will derive an approximate correction to the total H I mass.

BH90 found that the H I absorption is dominated by a broad component ($\Delta V \sim 120$ km s^{-1}) at $V_{\rm hel} = 3160$ km s^{-1} and a narrow component ($\Delta V \sim 70$ km s^{-1}) at $V_{\rm hel} = 3050$ km s^{-1}. Due to the near correspondence of these velocities with the systemic velocities of IC 694 and NGC 3690 (3080–3180 km s^{-1} and 3000–3080 km s^{-1}, respectively; BH90 and references therein) and because these two components are found in the absorption spectrum against *all* of the radio continuum sources, BH90 deduce that they are due to outer disk material from both IC 694 and NGC 3690 lying in the foreground, rather than near-nuclear gas clouds. This allows us to interpolate our H I column-density maps across the absorbing regions. This column density can then be used together with the ratio of the neutral gas absorbing column density to the spin temperature ($N_{\rm H\,I}/T_{\rm spin}$) given by BH90 to constrain $T_{\rm spin}$.

From the column densities given in Figure 2, we estimate a foreground column density of $N_{\rm H\,I} \approx 1$–2×10^{21} cm^{-2} due to the disk of IC 694. For the corresponding absorption component (i.e., the broad component at $V_{\rm hel} = 3050$ km s^{-1}), BH90 find $N_{\rm H\,I}/T_{\rm spin} \sim 3$–$8 \times 10^{19}$ cm^{-2} f_g K^{-1}, where f_g is the fraction of the radio continuum source covered by absorbing gas. Since BH90 find this absorption feature in the spectra of *each* continuum source in Arp 299, f_g must be near unity, yielding a spin temperature of 12–70 K. This is similar to the range found in our Galaxy (34–74 K; Kalberla, Schwarz, & Goss 1985). The lower range of temperatures are similar to the very low values of $T_{\rm spin}$

[9] These numbers increase to $L_B = 2.1 \times 10^9\ L_{\odot,B}$ (5%) and $L_R = 1.9 \times 10^9\ L_{\odot,R}$ (4%) if the background point sources are left in and a 0.5 mag arcsec^{-2} lower surface brightness threshold is used.

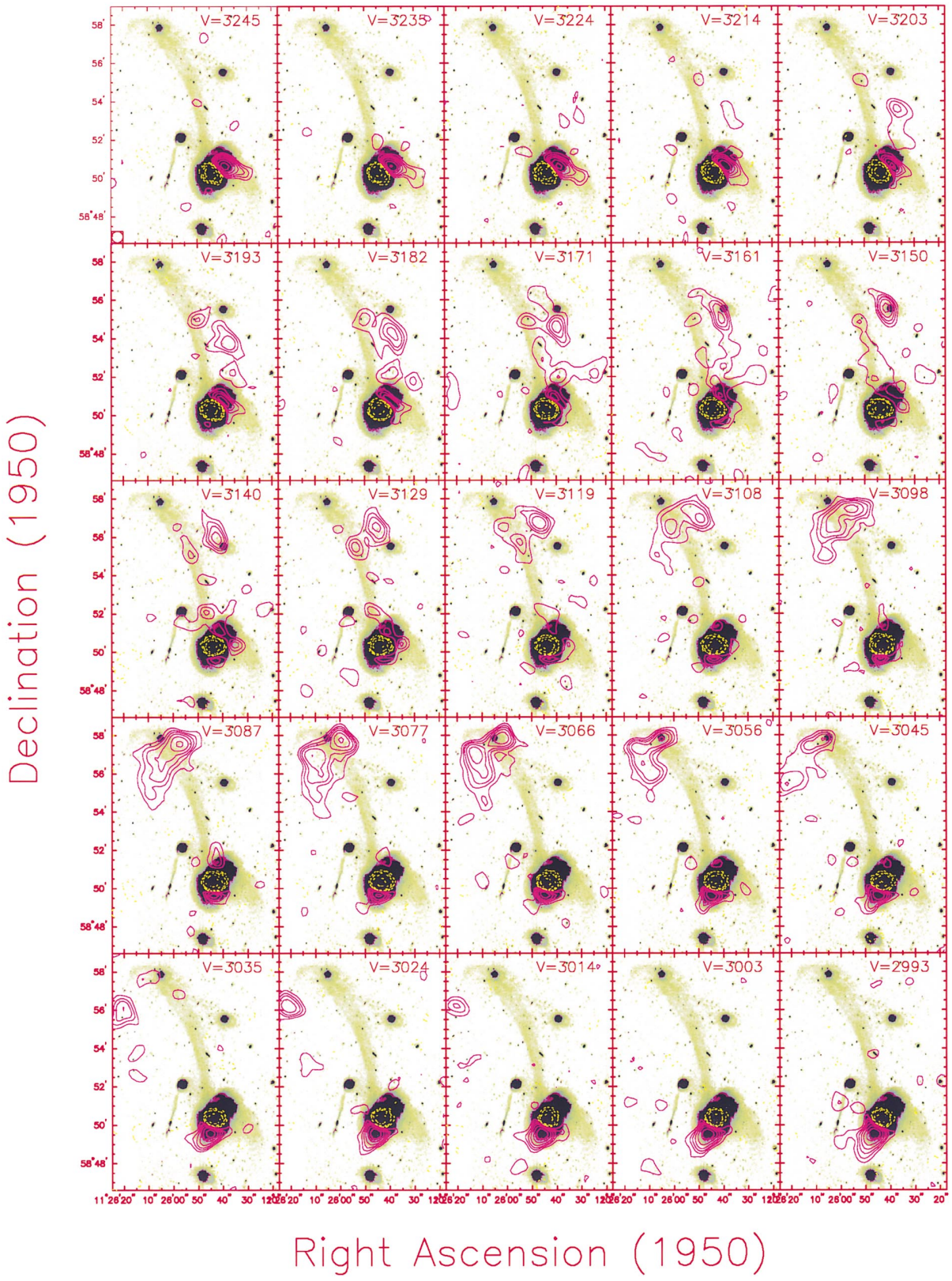

FIG. 8.—Channel maps of the tidal regions of Arp 299 contoured on the *B*-band image. The gray scales are drawn from $\mu_B = 28.5$ mag arcsec^{-2} (*white*) to 25 mag arcsec^{-2} (*black*). The more sensitive low-resolution H I cube is used at full velocity resolution (10.52 km s^{-1} channel width). The 35″ beam size is indicated in the lower left hand corner of the first panel, and each panel is labeled with the channel number and heliocentric velocity. Dotted yellow lines indicate negative contours, which are drawn at $1\ \sigma \times (-3, -5, -7, -10)$, where $1\ \sigma = 0.37$ mJy beam^{-1} is the single-channel noise level. Positive contours are drawn at levels of $1\ \sigma \times (3, 5, 7, 10, 15, 22.5)$. The lowest contour corresponds to a column density of 1×10^{19} cm^{-2}. Only channels showing H I emission from the tail are shown.

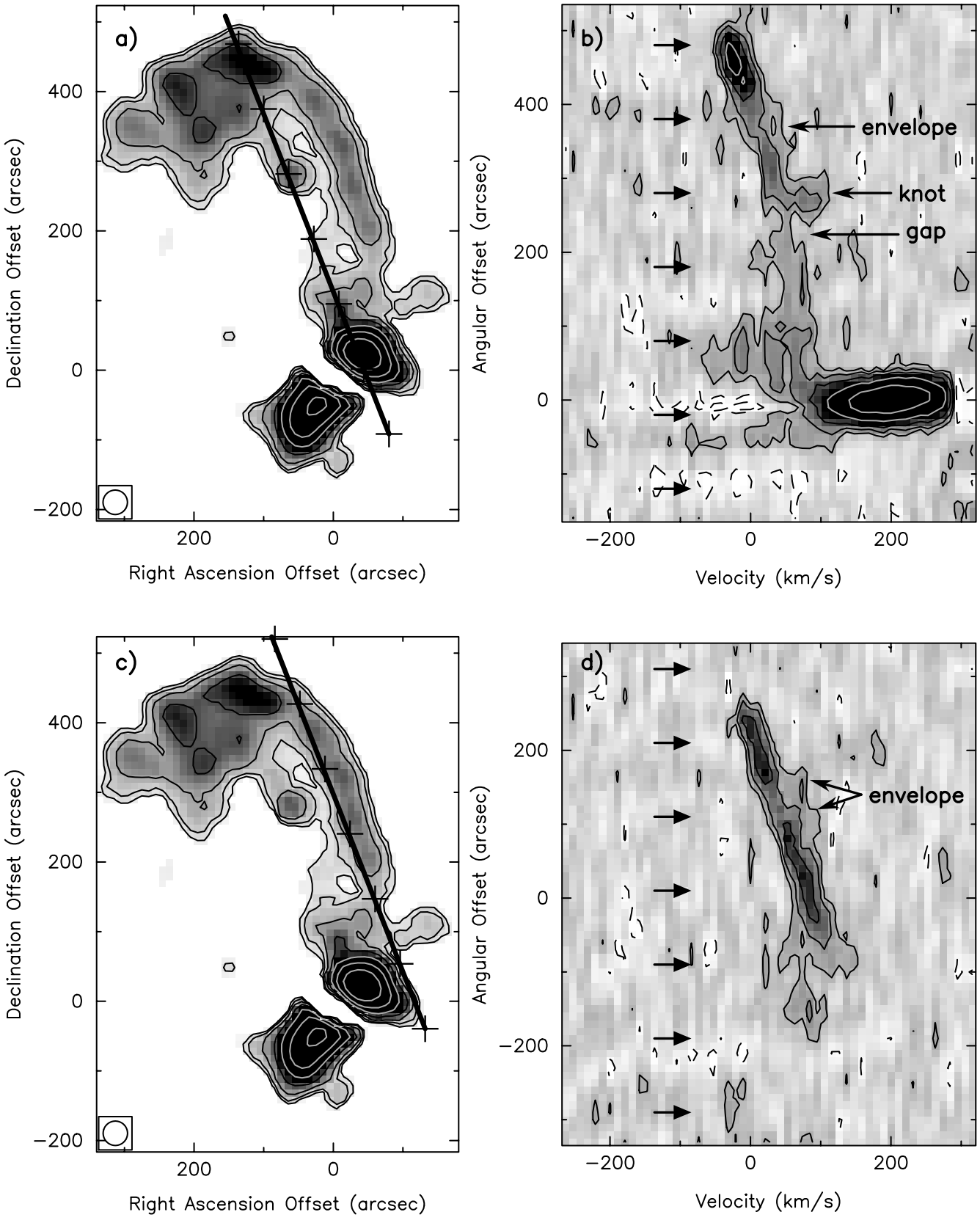

FIG. 9.—Position-velocity slices taken along both gaseous filaments. The left panels show the location of the slice on the low-resolution H I integrated intensity maps, while the right panels show the corresponding position-velocity profile. For the latter, distance along the slice is plotted along the *y*-axis, and velocity with respect to 3100 km s^{-1} is plotted along the *x*-axis. Crosses are drawn at intervals of 100″ along the slice in the left panel, and arrows indicate the corresponding locations in the right panel. Specific regions referred to in the text are labeled. Panels (*a*) and (*b*) show a position-velocity slice taken along the inner tidal filament. Panels (*c*) and (*d*) show a similar slice taken along the outer tidal filament.

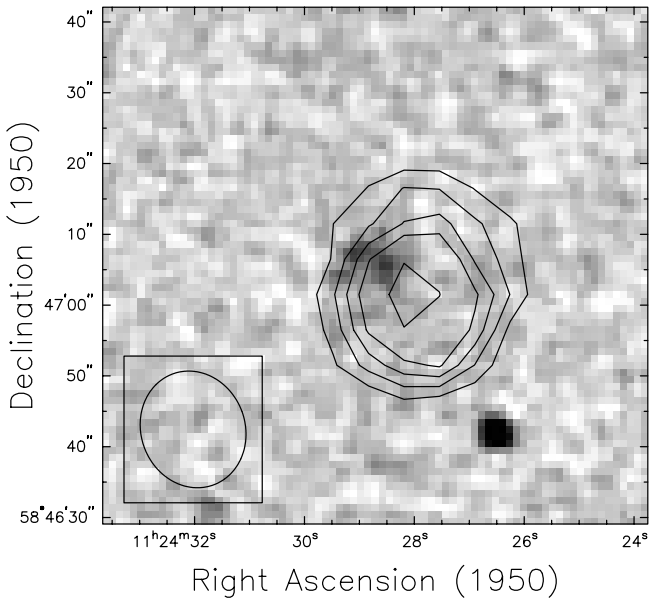

FIG. 10.—Gray-scale image of the companion to Arp 299, taken from Version II of the Digitized Sky Survey, with H I contours superposed. The higher resolution data are used with the 17″ × 15″ beam indicated by the ensquared ellipse to the lower left. H I column density contours are drawn at (5, 10, 15, 20, 30) × 10^{19} cm^{-2}.

($T_{spin} < 50$ K) found in the Magellanic stream (Kobulnicky & Dickey 1999) and the nearby galaxies NGC 247 and NGC 253 (Dickey, Brinks, & Puche 1992).

Using this range of spin temperatures and the measured N_{HI}/T_{spin} values from BH90 for the low-velocity absorption component ($V_{hel} = 3050$ km s^{-1}, $N_{HI}/T_{spin} = 1$–2×10^{19} cm^{-2} K^{-1}) we deduce a column density of $10^{20}-10^{21}$ cm^{-2} due to gas from NGC 3690. Adding these two contributions[10] gives an expected column density of 1–3 × 10^{21} cm^{-2} in front of the absorption region. Doubling these values to account for emission behind the continuum sources, we conservatively estimate an average column density in the absorbing region of 2 × 10^{21} cm^{-2}, corresponding to a "missing" H I mass of 2.2 × 10^9 $M_\odot$. This value is used to arrive at the "absorption corrected" M_{HI} value tabulated in Table 3. This total is very approximate and could easily be 2–3 times as large (see § 4.2).

3.5. H I *Detected Companion*

The H I observations uncovered a previously unknown and uncataloged companion to Arp 299 containing 8 × 10^7 $M_\odot$ of H I. This companion lies about 10′ west and 3′ south of Arp 299 (projected separation of $r = 140$ kpc) and has a systemic velocity of +145 km s^{-1} with respect to Arp 299. This region was not covered in our optical observations. An amorphous optical counterpart is found at this location on the XDSS image. The H I column density is contoured upon the XDSS image in Figure 10, and channel maps are shown in Figure 11.

We attempt to derive an optical luminosity for this companion from the Palomar Observatory Sky Survey (POSS) E plate of Version I of the DSS.[11] However, the number of counts from this source (log [counts] = 4.52) is lower than the levels over which calibration has been reliably determined (log [counts] = 4.8, $m_{POSS\,E} < 16$ mag). Extrapolating the faint end of the above curve to the observed number of counts gives a somewhat uncertain estimated magnitude of $m_{POSS\,E} = 17$ mag. Assuming an average value of $B-R = +1.0$ (e.g., van Zee, Haynes, & Salzer 1997), the absolute B magnitude of the H I companion is about $M_B = -15.4$.

The resulting global properties for the companion are given in Table 3. The optical appearance and H I properties of this system are similar to those of dwarf irregulars (Hoffman et al. 1996), and it is likely to have been a dwarf irregular companion of one of the progenitors. For comparison, it is about 20 times fainter and 30 times less gas-rich than the LMC (Tully 1988).

4. DISCUSSION

Although the differences between the optical and gaseous tidal morphology are bizarre, the tail kinematics and general morphology are very similar to the gas-rich tails of more classically understood mergers (e.g., Schweitzer 1978; van der Hulst 1979; Hibbard et al. 1994; HvG96), and the two main bodies certainly appear to be separate disk systems that have been strongly perturbed. It therefore seems that the tidal hypothesis—that these features arise as a result of two spiral galaxies falling together under their mutual gravitational attraction and merging due to dynamical friction (e.g., Toomre & Toomre 1972, hereafter TT72; Barnes & Hernquist 1996)—still provides the simplest explanation for the many peculiarities in this system.

Given this premise, we now aim to understand the gross characteristics of the encounter: what was the general encounter geometry (§ 4.1), and what were the approximate Hubble types of the progenitors (§ 4.2)? We explore possible explanations for the differences between the gaseous and stellar tidal features in § 4.3, although much of this discussion is deferred to a separate paper (Hibbard, Vacca, & Yun 1999, hereafter HVY99). In § 4.4 we examine what, if anything, the state of this system tells us about the conditions under which super-starbursts are initiated, leading to an ultraluminous infrared phase. Finally, in § 4.5 we discuss the lack of putative tidal dwarf galaxies in the outer tidal features.

4.1. *Nature of the Encounter*

The tail kinematics do not themselves determine the spin geometry of their progenitor. This is because the line-of-sight velocity fields of tidal features are often dominated by projection effects. This is particularly true of long filamentary tails, for which the space velocities will be oriented primarily perpendicular to our line of sight (leading directly to their large apparent lengths). Instead, we use the morphology of the tail to deduce the relative spin geometry between its progenitor disk and the orbital plane. In particular, only disks with a prograde spin geometry (i.e., a spin angular momentum roughly aligned with the orbital angular momentum of the two merging galaxies) can raise such long, drawn out features (TT72; Barnes 1988), and the

[10] There are additional absorption components seen in the H I absorption spectra obtained by BH90, but their association with OH emission features at similar velocities places them very close to the nucleus of IC 694 with a small covering factor, and they will therefore contribute very little to the total H I mass.

[11] Using the photometric solution available at http://www-gsss.stsci.edu/dss/photometry/poss_e.html.

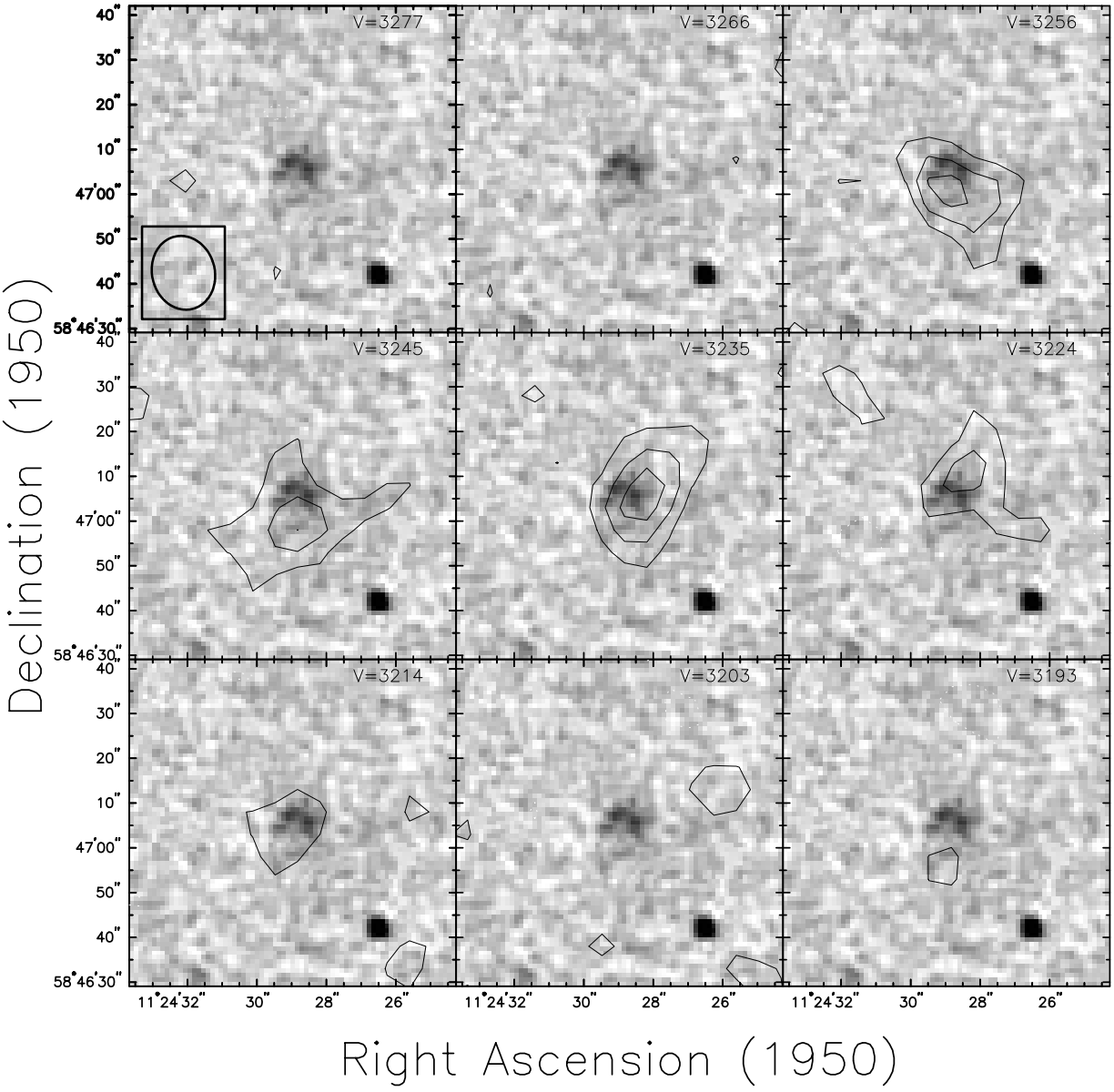

FIG. 11.—H I channel maps of the companion to Arp 299 contoured upon a gray scale of Version II of the Digitized Sky Survey. The higher resolution (17″ × 15″), full-velocity resolution ($\Delta v = 10.52$ km s^{-1}) H I data are used, with the spatial resolution indicated by the ensquared ellipse to the lower left of the first panel. Contours are drawn at 1 $\sigma \times (-3, 3, 5, 7)$, where 1 $\sigma = 0.20$ mJy beam^{-1} is the single-channel noise level, corresponding to a column density of 9.2×10^{18} cm^{-2}.

progenitor of the northern tail must have had just such a prograde spin orientation.

Further, since tidal tails remain close to the original spin plane of the disk from which they are extracted (TT72) and the observed tail in Arp 299 emerges at nearly right angles to the disk of IC 694, we conclude that IC 694 could not have generated this feature. The tail must therefore have arisen from NGC 3690. Similarly, the lack of any narrow drawn-out features near the plane of the disk of IC 694 suggests that this system experienced the encounter in a highly inclined or retrograde sense. Such encounters provoke a much milder kinematic response in a disk (e.g., TT72; White 1979; Noguchi 1991), accounting for the survival of the disk morphology and kinematics of IC 694 so late into the encounter. This spin geometry agrees with the kinematics of the inner regions derived from Hα emission-line kinematics, which show that IC 694 and NGC 3690 rotate in opposite directions (Augarde & Lequeux 1985; Hibbard, Bland-Hawthorn, & Tully 1999a). Further, the systemic velocities for the two nuclei ($V_{\rm hel} \approx 3135$ km s^{-1} for IC 694 [§ 3.1] and $V_{\rm hel} \approx 3040$ km s^{-1} for NGC 3690 [§ 3.4]) give them the proper sense of motion for the inferred spin geometry—the nuclei rotate about each other opposite the direction that the disk of IC 694 rotates.

The morphology and kinematics of the ionized gas in Arp 299 has been mapped with a Fabry-Perot interferometer (Hibbard et al. 1999a), showing that there is spatial and kinematic continuity between the outer H I disk all the way inward to source A. This implies that the entire disk structure belongs to IC 694; i.e., the H I is not distributed in a settled disk in rotation about both systems, as suggested by Stanford & Wood (1989). Further, these observations reveal

that NGC 3690 and sources B and C′-C are kinematically distinct from the IC 694 disk, as expected from the inferred prograde-retrograde spin geometry.

From the redshifted velocities along most of the outer tail and the fact that the tail should be predominantly in expansion along most of its length (Hibbard & Mihos 1995), we deduce that the tail curves away from us and should connect to the main bodies from behind. In this case, the decrease in velocities seen at the very base of the tail in Figure 9*b* (third arrow from the bottom in both figures; see also northern region of upper right panel in Fig. 2), indicates that the material at the base of the tail has reached its apocenter and is falling back to smaller radii (e.g., Hibbard et al. 1994; Hibbard & Mihos 1995). Similarly, the broad range of velocities seen for the minor-axis clump of H I (Fig. 3) suggests that this material is part of the northern tail connecting back to its progenitor, NGC 3690. If there is more H I associated with the disk of NGC 3690, it would be difficult to disentangle from the emission due to the southwest portion of the disk of IC 694 and the central H I absorption.

Finally, the western plume may be disk material from IC 694 that was perturbed during an earlier pericentric passage of the two galaxies about each other or by the passage of the compact northwest spheroidal (MCG +10-17-2a). Since tidal material tends to lie within the plane it occupies at the time it is raised (TT72), the distribution of this gas should reflect the plane of the disk of IC 694 at an earlier stage of the merger, perhaps at an early pericentric approach. The fact that this plane is different from the present plane suggests that the angular momentum of the disk was changed during the encounter, evidence for which is also seen in the Hα Fabry-Perot maps at smaller radii.

These observations show the power of sensitive H I and deep optical imaging of peculiar systems. It has long been believed that Arp 299 is in a very early stage of its interaction, given the relative youth of the ongoing starburst ($\lesssim$20 Myr; Vacca et al. 1999; Meurer et al. 1995; Stanford 1989; Nakagawa et al. 1989; Augarde & Lequeux 1985). The apparent lack of tidal features in their H I observations led Standford & Wood (1989) to conclude that the outer tidal H I had quickly settled into a disk configuration early in the encounter. The discovery of the 180 kpc tidal tail obviously changes this conclusion. It also requires the interaction to be quite old. Taking a typical rotation speed of 240 km s^{-1} from the inner disk kinematics and saying that this is the maximum velocity available to the tidal debris, we calculate that the tail has taken at least 750 Myr to form. Therefore *the dynamical age of the merger is substantially larger than the age of the present starburst*. Arp 299 is not unique in this sense (e.g., Mihos & Bothun 1998), and this cautions against using the age of the starbursts to age-date an interacting system, as is frequently done for the peculiar star-bursting objects at high redshift. Further, it is possible that Arp 299 experienced several short bursts of elevated star formation since the tail was first launched. In that case, the accumulated burst populations would not be coeval, but would show a spread of ages, and the expected age signatures in the resulting remnant would be much less pronounced then is often presumed (e.g., Silva & Bothun 1998).

4.2. *Nature of the Progenitors*

Now that we have used the H I kinematics to establish approximate associations between the different kinematic features and their progenitors, we attempt to divide the gas content and *B*-band luminosities between the two systems. We will then use these global quantities in concert with the statistical properties of normal Hubble types in an attempt to deduce the approximate Hubble types of the progenitors. It should be noted that not only are there significant uncertainties inherent in apportioning the gas and light between the two systems, but there is also a notoriously large scatter in global properties along the Hubble sequence and a further uncertainty due to conversion between gas phases and from gas into stars in the context of the ongoing starburst. However the following should provide a very rough guess for the likely progenitors.

As mentioned above, we associate the H I from the tidal tail and minor axis clump with NGC 3690 ($M_{\rm H\,I} = 3.5 \times 10^9\ M_\odot$) and the inner disk and W plume of H I with IC 694 ($M_{\rm H\,I} = 6.2 \times 10^9\ M_\odot$). Simple dynamics suggest that less than one-half of the disk can be ejected into a tidal tail and that most of this quickly falls back onto the merging system (Hibbard & Mihos 1995). This suggests a total H I content of 2–3 $\times\ M_{\rm H\,I,tidal} = (7\text{–}10) \times 10^9\ M_\odot$ for NGC 3690. However, this value is already more than the combination of the tidal H I and the absorption correction ($5.7 \times 10^9\ M_\odot$). This discrepancy suggests that our absorption correction was probably too conservative (§ 3.4). Rather than trying to account for gas that we have no firm measure of, we simply associate all of the absorption-corrected gas ($2.2 \times 10^9\ M_\odot$) with NGC 3690 and remark that the H I masses for both IC 694 and NGC 3690 are likely significantly underestimated. Using the ^{12}CO (1–0) observations of Casoli et al. (1999), we associate the "widespread" molecular gas and that near source A with IC 694, the molecular gas near source B with NGC 3690, and split the molecular gas from the overlap region (C′-C) between the two systems. Total gas masses are calculated by adding the atomic and molecular hydrogen gas masses and multiplying by 1.36 to account for He. Finally, the individual *B*-band luminosities are estimated by summing the light over irregular polygons drawn around each system and are therefore also very approximate. The results of this division are given in Table 4, and we use these values in concert with the following statistical properties of normal Hubble types:

1. $M_{\rm H_2}/M_{\rm H\,I}$ increases toward earlier Hubble types (Young & Knezek 1989; Young & Scoville 1991). The high values in Table 4 suggests progenitor types later than Sab and earlier than Sc. They also argue against low surface brightness progenitors (de Blok & van der Hulst 1998).
2. $M_{\rm H\,I}/L_B$ increases toward later Hubble types (Roberts & Haynes 1994; Giovanelli & Haynes 1990). The high values in Table 4 suggest types later than Sa (Wardle & Knapp 1986; Bregman, Hogg, & Roberts 1992) and later than Sb (Roberts & Haynes 1994).
3. The large mass of H I suggests types later than Sa (Huchtmeier & Richter 1988; Bregman et al. 1992) and earlier than Sc (Huchtmeier & Richter 1988; Giovanelli & Haynes 1990).
4. The large values of $M_{\rm H_2}$ and $M_{\rm gas}/L_B$ suggest types later than Sa (Hogg, Roberts, & Sandage 1993).
5. The large values of $M_{\rm H_2}/L_B$ favor types later than Sab (Lees et al. 1991; Bregman et al. 1992).

These consideration suggest progenitor types of Sab-Sc for both systems—an earlier type for IC 694 and a later type for the NGC 3690. This view is supported by high-

TABLE 4

GLOBAL QUANTITIES

Quantity	Units	Total	IC 694	NGC 3690
L_B	$L_{\odot,B}$	4.5×10^{10}	2.8×10^{10}	1.7×10^{10}
$M_{\rm H\,I}$	$M_\odot$	1.18×10^{10}	6×10^9	6×10^9
$M_{\rm H_2}$ [a]	$M_\odot$	1.7×10^{10}	1.1×10^{10}	6×10^9
$M_{\rm gas}$ [b]	$M_\odot$	3.9×10^{10}	2.3×10^{10}	1.6×10^{10}
$M_{\rm H\,I}/L_B$	$M_\odot\ L_{\odot,B}^{-1}$	0.3	0.2	0.4
$M_{\rm H_2}/L_B$	$M_\odot\ L_{\odot,B}^{-1}$	0.4	0.4	0.4
$M_{\rm gas}/L_B$	$M_\odot\ L_{\odot,B}^{-1}$	0.9	0.8	0.9
$M_{\rm H_2}/M_{\rm H\,I}$		1.4	1.8	1.0
$L_{\rm IR}$ [c]	$L_{\odot,\rm bol}$	7.9×10^{11}		
$L_{\rm IR}/L_B$		18		
$L_{\rm IR}/M_{\rm H_2}$	$L_\odot\ M_\odot^{-1}$	69		

[a] From Casoli et al. (1999), converting to our distance and a CO-to-H_2 conversion factor of 3×10^{20} cm^{-2} (K km s^{-1})$^{-1}$. We have divided the gas located at the overlap region $C-C'$ equally between IC 694 and NGC 3690 and assigned the "widespread" emission to IC 694.

[b] Total gas mass corrected for the presence of He: $M_{\rm gas} = (M_{\rm H\,I} + M_{\rm H_2}) \times 1.36 \times M_{\rm H\,I}$.

[c] Far-infrared luminosity over the range 8–1000 μm, from Sanders et al. (1991).

resolution (1″) NIR imaging of the brightest sources at 2.2 μm by Wynn-Williams et al. (1991). In that study, the light profiles of the brightest NIR sources within Arp 299 were compared with stellar profiles taken immediately before and after the on-source exposures. It was found that source A is clearly resolved, with a FWHM of 460 pc (correcting to our adopted distance of 48 Mpc), while the point sources within NGC 3690 are found to have cores that are indistinguishable from stars, implying that they have diameters of less than 230 pc at 2.2 μm. These considerations suggest a more extended bulge for IC 694 than for NGC 3690, lending further support to an earlier type for the former and a later type for the latter. We therefore suggest progenitor types of Sab-Sb for IC 694 and Sbc-Sc for NGC 3690.

In summary, we believe that Arp 299 results from a prograde-retrograde encounter between a gas-rich Sab-Sb (IC 694) and Sbc-Sc (NGC 3690) that occurred 750 Myr ago. We estimate that the system will fully merge on a timescale somewhere between a crossing time $d/v_{\rm max}$ and an orbital period $\pi d/v_{\rm max}$ at the present separation d of 4.7 kpc, or sometime between 20–60 Myr from now (for a rotational speed of 240 km s^{-1}).

4.3. *Explanations for Outer Tidal Morphology*

The differences between the gaseous and stellar tidal morphologies were very unexpected. Displacements between optical and gaseous tails or bridges are not unheard of (e.g., NGC 4725/47, Wevers et al. 1984; Arp 295, HvG96; NGC 7714/5, Smith, Struck, & Pogge 1997; NGC 2782, Smith 1994); nor are gaseous tidal tails or streamers with little, if any, starlight (e.g., NGC 2444/5, Appleton et al. 1987; M81, Yun et al. 1994); nor are stellar tails or plumes with no H I (e.g., NGC 3921, HvG96; Arp 105, Duc et al. 1997; NGC 2782, Smith 1994). There are even examples of much less extreme "bifurcated" gaseous tails, in which a single tidal tail appears to split near its base into parallel H I filaments, both of which have similar kinematics (e.g., M81 Yun et al. 1994; NGC 3921, HvG96; NGC 2535/6, Kaufman et al. 1997; NGC 4038, Hibbard, van der Hulst, & Barnes 1999c). What is unique in Arp 299 is that all these effects occur at once—there is a tail that is bifurcated along almost its entire length, with one filament gas-rich and the other gas-poor, and a striking anticorrelation between the gaseous and stellar filaments where the filaments join. In this subsection, we investigate possible explanations for each of these characteristics in turn.

4.3.1. *Gas-Rich Outer Filament*

The high $M_{\rm H\,I}/L_B$ ratios found for the outer filament are rather extreme, with peaks greater than 10 $M_\odot\ L_\odot^{-1}$ and a mean of approximately 4 $M_\odot\ L_\odot^{-1}$. However they are similar to the values found in other gaseous tidal extensions (e.g., Arp 143, Appleton et al. 1987; NGC 2782, Smith 1994; NGC 7252, Hibbard et al. 1994). In these systems, the gas-rich extensions appear to be due to the fact that $M_{\rm H\,I}/L_B$ is an increasing function of radius in spiral galaxies (Wevers, van der Kruit, & Allen 1986)[12]. Since the outermost (gas-rich) regions of the disk become the outermost regions of the resulting tidal tails (TT72), gas-rich extensions to optical tails are to be expected. The higher dispersion of outer disk stars with respect to the gas (van der Kruit 1988) and the finite lifetimes of the most luminous stars will exacerbate this effect, leading to further increases in $M_{\rm H\,I}/L_B$ in the outer regions (HvG96).

However, Arp 299 is quite different from the above mentioned systems in that it is not just the outermost regions that are gas-rich—the gas-rich filament appears to extend all the way back to the main body, running parallel to the optical tail. That is, it appears to cover a very broad range of radii. So the first question we wish to address is whether such a feature can arise because of a combination of dynamical and projection effects that cause the gas-rich outer regions to be projected adjacent to the optically brighter inner regions.

We believe that answer to this question lies in the dynamical development of tidal tails, as demonstrated so vividly by TT72. These authors emphasized that tails are not linear structures, but actually two dimensional

[12] This is usually expressed as the well-known fact that H I disks often extend further than optical disks; see, e.g., Bosma 1981; Wevers et al. 1986; Cayatte et al. 1994; Broeils & van Woerden 1994.

"ribbons" twisting through space. In particular, Fig. 2 of TT72 shows that the outermost edges of the ribbon come from the outermost radii of the original disk, while middle regions come from intermediate radii, etc.; hence, the outer disk material forms a "sheath" around the inner disk material along its entire length. Therefore it is possible that a lateral twist may cause the outer edge of the ribbon to lie in a different plane from the inner regions, i.e., for the most gas-rich regions to appear in a different plane from the less gas-rich, optically brighter regions.

The models also show that the material from different radii form continuous structures in space and velocity and hence that the resulting tidal features will necessarily be continuous in space and velocity as well (Barnes 1988; Hibbard & Mihos 1995). But while the parallel filaments of Arp 299 appear to be kinematically continuous, they appear morphologically distinct, or bifurcated. We suggest that the bifurcation arises because of a preexisting warp in the outer regions of one of the disk. This suggestion comes from our recent attempts to match the tidal morphology and kinematics of the northern tail using N-body simulations. In our preliminary trials (using only 4096 particles per galaxy), we can rather easily match either the morphology and kinematics of the outer tidal filament and N clump or the kinematics of the inner filament and morphology of the stellar tail. However, we have been unable to match both features simultaneously with a single disk orientation and viewing angle. This leads us to suspect that the disk of NGC 3690 was initially warped (as is often the case for disk galaxies; Bosma 1991). In this case, the outer, optically fainter regions will be pulled off along one plane (resulting in the outer tidal filament), while the regions from smaller radii will move primarily in a different plane (resulting in the inner filament). A similar explanation may account for the less extreme bifurcated structures seen in other tidal tails (e.g., M81, Yun et al. 1994; NGC 3921, HvG96; NGC 2535/6, Kaufman et al. 1997; NGC 4038, Hibbard et al. 1999c).

However, this projection effect does not explain the low H I content of the optical tail in Arp 299. Although the less extreme radii of spirals have a lower $M_{\rm H\,I}/L_B$ than the outer regions, they still have significant quantities of H I. We therefore seek a separate explanation for this feature.

4.3.2. *Gas-Poor Inner Filament*

For the original disk to give rise simultaneously to a gas-rich outer filament and a gas-poor optical filament would require a special H I radial distribution—one in which the gaseous disk had a low column density within the stellar disk but was very gas-rich beyond this. Such distributions are indeed seen in some early type galaxies, especially SB0s (van Driel & van Woerden 1991). However, two facts lead us to suspect that this is not a viable explanation for Arp 299. The first is that such systems usually have an order of magnitude less H I than observed in the tidal tail of Arp 299 (which itself is less than half of the original gas content). The second is that the starlight in such systems is dominated by an extended central bulge, which the NIR observations appear to rule out for NGC 3690 (§ 4.1).

Another factor leading us to consider other explanations is that Arp 299 is one of a number of peculiar starburst galaxies exhibiting curious displacements between tidal H I and starlight. Further, the five systems that exhibit the most dramatic displacements (M82, Yun, Ho, & Lo 1993; NGC 4631/4656, Weliachew, Sancisi, & Guelin 1978; NGC 520, HvG96; Arp 220, Yun, Hibbard, & Scoville 1999, HVY99; and Arp 299) also host massive nuclear starbursts with associated powerful outflows that extend many kiloparsecs from the nuclear regions ("superwinds," e.g., Heckman, Lehnert, & Armus 1993; Lehnert & Heckman 1996), and in each case the tidal H I shows a displacement or anticorrelation along the direction of the expanding hot superwind fluid. This leads us to suspect a possible interaction between the expanding wind fluid and the tidal debris (see also Chevalier & Clegg 1985; Yun et al. 1993; Heckman et al. 1993; Dahlem et al. 1996).

This issue is covered in more detail in HVY99, and here we just discuss the specific details of Arp 299. In this system the evidence for an expanding superwind comes from the morphology and kinematics of the optical emission-line gas (Armus et al. 1990) and the X-ray observations of Heckman et al. (1999). In the latter, the soft X-ray emission from hot gas is oriented perpendicular to the harder X-ray emission from discrete X-ray sources associated with the starburst. The hot gas emission is elongated roughly along the minor axis of IC 694, extending to a radius of order 25 kpc (Heckman et al. 1999). Since the observed X-ray emission represents just the hottest, densest portions of the adiabatically expanding wind (Wang 1995), the full extent of the wind should extend well beyond this.

The mechanical effect of such a wind may be evidenced in the increased column density and velocity dispersion of the H I knot in the inner filament ($r \approx 60$ kpc), which might be due to the wind's ram-pressure effects. The wind might also account for the high-velocity envelope of gas seen in Figure 9 and the high-velocity dispersion regions seen on the southern end of the N clump in Figure 7*d*. However, we do not believe that the wind's ram pressure has pushed the gas fully out of the inner filament and into the outer filament. Such action should significantly change the kinematics of the gas, whereas the kinematics of the gas within both filaments is nearly identical. Instead, we suspect that the superwind affects the ionization state of the gas in one of two ways: either directly by shock ionization or indirectly by clearing a sight line from the tidal tail to the nuclear starburst, allowing UV photons from the young stars to escape these regions and reach parts of the tail. Calculations carried out in HVY99 suggests that both scenarios are in principle capable of affecting gas at the observed column densities and distances, although there is insufficient evidence to discriminate between them.

Whether the "missing" H I has been ionized or not is subject to observational investigation. The expected emission measure in convenient units is

$$\mathrm{EM} = 0.42\ \mathrm{cm}^{-6}\ \mathrm{pc}\left(\frac{N_{\rm H\,I}}{2\times 10^{20}\ \mathrm{cm}^{-2}}\right)^2\left(\frac{10\ \mathrm{kpc}}{dL}\right)^2, \quad (1)$$

where $N_{\rm H\,I}$ is the missing column density of H I and dL is the line-of-sight depth of the H I column. If the gas has a clumpier distribution, then there should be some higher density peaks with emission measures well above these levels. These emission measures are within the capabilities of modern CCD detectors (e.g., Donahue, Aldering, & Stocke 1995 obtained 0.3 cm^{-6} pc in NGC 4631), and such emission would be well worth looking for.

4.3.3. *Gas/Light Anticorrelation in the* N *Clump*

The main problem with the above scenarios is that neither can explain the H I and optical anticorrelation at the

end of Arp 299 tail, whereby there is a local minima in the H I column density where the optical tail crosses the N clump, and local maxima to either side of this (Fig. 7*b*). The expanding galactic wind or photoionization cone should have no idea where the optical tail lies. In HVY99, we suggest that the outer H I from the warped disk is already in a highly ionized phase because of its low density and the intergalactic UV field. In this environment, we suggest that the additional ionizing radiation due to evolved sources within the stellar tail itself, such as late-B stars and/or white dwarfs, increases the ionization fraction of the local gas over that of the tidal gas without accompanying starlight. The lower neutral fraction is then seen as a drop in the neutral gas column density. A simple calculation is carried out in HVY99 that suggests that this process is in principle feasible if the gas in the N clump has a line-of-sight thickness $\gtrsim 25$ kpc. In that case, the expected emission measure ($\lesssim 0.02$ cm^{-6} pc) is well below what is observable with current technology.

4.3.4. *Outer Morphology: Conclusions*

These explanations are somewhat unsatisfactory, because we need three separate mechanisms to explain the three puzzling characteristics: a warped H I disk to explain the parallel tidal filaments, a starburst wind or unusual initial H I distribution to explain the lack of H I within the optical filament, and an increased ionization fraction in the gas due to the presence of the stellar tail to explain the anti-correlation between the H I and optical light in the N clump. Whatever their cause, these observations point to some important differences occurring between gas and stars during the formation of some tidal tails.

4.4. *Conditions for Luminous Infrared Phase*

A main objective of our studies on the atomic gas in IR-luminous galaxies ($L_{\rm IR} > 3 \times 10^{11}\ L_\odot$, Hibbard & Yun 1996, 1999) and the molecular gas in the less IR-luminous systems of the Toomre Sequence (Yun & Hibbard 1999) is to investigate the conditions necessary for fueling a highly elevated period of star formation. Certainly, a high gas content is one of the prerequisites for fueling such large starbursts (Sanders et al. 1988). We are interested in knowing whether all mergers between gas-rich galaxies pass through such a phase or if there are requirements on the progenitor properties or encounter characteristics to trigger such bursts. To gain some insight into how this efficient mode of star formation is triggered in Arp 299, we draw upon statistical studies of luminous IR galaxies and the results of numerical simulations.

The tight correlation between molecular gas column density ($\Sigma_{\rm H2}$) and $L_{\rm IR}$, especially when compared with the much looser correlation of gas mass with $L_{\rm IR}$, shows that IR-luminous starbursts are always precipitated by a corresponding increase in the nuclear column densities of molecular gas (Scoville et al. 1994; Solomon et al. 1997; Kennicutt 1998; Taniguchi & Ohyama 1998; Yun & Hibbard 1999). The CO observations of Arp 299 (Sargent & Scoville 1991; Aalto et al. 1997; Casoli et al. 1999) show that the highest column densities in Arp 299 occur at the nucleus of IC 694, with $\Sigma_{\rm H2}$ over 3 times higher than at the nucleus of NGC 3690. Additionally, HCN mapping observations of Arp 299 (Aalto et al. 1997; Casoli et al. 1999) show that the vast majority of the very dense gas ($n > 10^4$ cm^{-3}) is associated with the nucleus of IC 694.

Since the two progenitor galaxies appear to be of nearly equal mass and of similar total gas content (Table 4), we suggest that the reason there has been so much more gaseous dissipation toward the nucleus of IC 694 is its retrograde spin geometry (see also Sanders et al. 1988). In such encounters, the gas within the disk is not pulled into tidal bridges and tails, but remains in the disk where it feels the perturbation from the second system alternately pulling it outward and pushing it inward during an orbit (e.g., TT72; White 1979; Noguchi 1991). This excites large epicyclic motions in the gas, which in turn lead to higher collision rates (e.g., Olson & Kwan 1990; Noguchi 1991) and hence to more gaseous dissipation.

This suggestion would seem to be at odds with the results from numerical simulations, which find only a moderate dependence of gaseous dissipation and/or star formation activity on the encounter spin geometry (e.g., Mihos & Hernquist 1996). Moreover, these simulations invariably have the starbursts occurring only when the nuclei finally coalesce, while in Arp 299 (and other IR-luminous mergers, Murphy et al. 1996; Mihos & Bothun 1998), the nuclei are still well separated ($d > 4.7$ kpc). A possible solution to these concerns is found in the simulations of Noguchi (1991), who stresses the episodic nature of starbursts in mergers (see also Olson & Kwan 1990). Noguchi notes that while the maximum enhancement of activity is not strongly dependent on the spin geometry of the encounter, the time evolution of the activity is. In particular, his prograde-retrograde encounter produces a longer period of enhanced activity over other spin combinations and also leads to a slower coalescence of the nuclei. As a result, the cloud collision rate is still significantly increased as the nuclei separate (see his Fig. 9). This model predicts that the most luminous phase of Arp 299's starburst is still in the future, in which case this merger is predicted to outshine even Arp 220.

However, the numerical simulations are necessarily ad hoc in nature, and the microphysics of hydrodynamics (e.g., smoothed particle hydrodynamics as in Mihos & Hernquist 1996 versus sticky particle as in Noguchi 1991), star formation, and "feedback" (energy input back into the interstellar medium because of star formation) is poorly understood. Therefore, before drawing too many inferences from the simulations, it would be prudent first to test the numerical formalisms for star formation, dissipation, and feedback by direct comparison with real systems. Until simulations can reproduce starbursts occurring at the times and locations as observed, we must be cautious when extrapolating their results too far into the future.

The *observational* fact that systems can experience much of their star formation when the nuclei are well separated has important ramifications for the structure of the resulting remnant. In particular, stars are dissipationless and cannot radiate their orbital energy away. Therefore, stars that form while the nuclei are well separated will be spread over a larger range of radii in the resulting remnant than those that form when the nuclei are practically merged. This population can experience violent relaxation (e.g., Barnes 1992; Barnes & Hernquist 1996), resulting in an extended dynamically hot population. The resulting remnant will have a much more regular luminosity profile than a merger in which the gas all sinks to the very center of

the potential before forming stars (cf. concerns raised in Mihos & Hernquist 1994).

4.5. *Lack of Tidal Dwarfs*

The widespread lack of a small-scale correlation between optical and gaseous density enhancements within the tidal tail was unexpected. In previous H I and optical observations of six double-tailed merging systems (van der Hulst 1979; Hibbard & van Gorkom 1993; HvG96; Hibbard et al. 1994), five dwarf-galaxy–like concentrations of gas, light, and Hα emission appear entrained within tidal tails *and* coincident with distinct features in the optical color maps and the H I velocity dispersion maps. These concentrations have been interpreted as "tidal dwarf galaxies" forming out of the expanding tidal material (see also Schweitzer 1978; Mirabel, Dottori, & Lutz 1992; Duc et al. 1997; Malphrus et al. 1997), an idea that has been supported by numerical simulations (Barnes & Hernquist 1992, 1996; Elmegreen, Kaufmann, & Thomasson 1992; Hibbard & Mihos 1995). In addition to these dwarf-sized concentrations, the previously observed tidal tails often contain numerous knots of gas, light, and star-forming regions (see also Hutchings 1996; Hunsberger, Charlton, & Zaritski 1996; Mihos & Bothun 1998). We therefore fully expected similar features to appear in a tidal feature as long and as massive as that seen in Arp 299.

However, the optical tail of Arp 299 is remarkably smooth and featureless (Fig. 5). There are a number of point sources falling upon the optical tail, but the surface density of such points is similar to that of point source elsewhere in the field. Their colors are generally quite red ($B-R > 1.7$; Fig. 7*a*), and most are probably background galaxies. And while there is considerable structure within the H I tail, there are no H I peaks with a corresponding enhancement in the underlying starlight (Fig. 7*b*). Further, there are only three regions that exhibit a significant (>20%) increase in the H I velocity line width (indicated in Fig. 7*d*)—along the southern edge of the N clump and at the H I knot in the inner tidal filament (§ 3.3)—and these features do not correspond to any notable features in the optical images or color maps.

To investigate this question further, we estimate the importance of self-gravity within the tail by comparing the luminous mass ($M_{\rm lum}$) to the dynamical mass ($M_{\rm dyn}$). The luminous mass is estimated by adding the gas mass and the stellar mass. The latter is estimated from the *B*-band surface brightness and adopting a stellar mass-to-light ratio of $(M/L)_B = 2\,M_\odot\,L_\odot^{-1}$, characteristic of stellar disks (Bottema 1993). The dynamical mass is calculated via $M_{\rm dyn} = 1.76 \times 10^6\,M_\odot \times \sigma_{\rm H\,I}^2 \times r_{1/2}$ (Binney & Tremain 1987; see also Kaufman et al. 1997), where $r_{1/2}$ is the FWHM radius of the beam (~1.9 kpc for the high-resolution data). This will overestimate the effects of self-gravity if (1) the line-of-sight dimension of the tail is larger than the beam width (~3.8 kpc), in which case the above prescription overestimates the stellar mass, and (2) the stars contribute significantly to $M_{\rm lum}$ and have a velocity dispersion greater than $\sigma_{\rm H\,I}$ (e.g., van der Kruit 1988). Since we suspect both of these conditions to hold, our calculation of $M_{\rm lum}/M_{\rm dyn}$ should be a stringent upper limit. We derive a lower limit to $M_{\rm lum}/M_{\rm dyn}$ by setting $M_{\rm lum} = M_{\rm gas}$.

Using the high-resolution data, we find that $M_{\rm lum}/M_{\rm dyn} < 0.3$ everywhere, with the highest values on the brighter optical peaks of the inner tidal filament.[13] The peaks in the H I column density along the outer filament and in the N clump have $0.2 < M_{\rm lum}/M_{\rm dyn} < 0.3$, and the H I knot in the inner filament has $0.1 < M_{\rm lum}/M_{\rm dyn} < 0.2$. For comparison, the tidal dwarfs in the tail of NGC 7252 (Hibbard et al. 1994), NGC 3921 (Hibbard & van Gorkom 1993; HvG96) and NGC 4038/9 (Mirabel et al. 1992) have $0.50 \lesssim M_{\rm lum}/M_{\rm dyn} \lesssim 1$. Therefore, Arp 299 lacks the potentially self-gravitating dwarflike concentrations seen in other tailed systems, and we conclude that tidal dwarf formation is not a ubiquitous process.

This suggests that the formation of such substructures may depend on factors other than the ability to raise a decent sized tail. We note that other tidal tails that contain candidate tidal dwarf galaxies have similar gas column densities as those in the tail of Arp 299 but have optical tails that are about 2 mag arcsec^{-2} brighter. Additionally, in these systems the gas and optical material coincide. Both of these factors increase the underlying mass density within the tail. Further, since the gas in observed tidal dwarfs makes a significant contribution to the dynamical mass ($M_{\rm gas}/M_{\rm dyn} \approx 0.5$), it may be the case that whatever process removes the H I from the inner tidal filament (see § 4.3.2) also suspends the dwarf formation process.

Whatever the explanation, the present observations suggest that one should be cautious about simply measuring the mass or light contained within the highest gas column density contours or optical isophotes and calling these concentrations distinct entities.

5. CONCLUSIONS

1. A new tidal tail has been discovered in the ongoing merger Arp 299. The tail stretches 180 kpc to the north and must have taken at least 750 Myr to form. This is much longer than the age of the current starburst, suggesting that the starburst and merger clocks start at different times and run at different rates. If the present starburst began when the tidal tail was first launched, the spread of ages in the resulting remnant will be much larger than is usually assumed.

2. What had previously been interpreted as a single rotating gaseous disk surrounding the two merging systems is shown to be a gaseous disk associated with the eastern system, IC 694. The kinematic information in concert with the optical morphology allows us to deduce that NGC 3690 experienced a prograde encounter, while IC 694 experienced a retrograde encounter. From the cold gas contents and NIR morphologies, we suggest late-type progenitors for both systems (Sab-Sb for IC 694, Sbc-Sc for NGC 3690).

3. The observations show that Arp 299 is experiencing an IR-bright starburst while the nuclei are still well separated ($dr \gtrsim 4.7$ kpc). We suggest that this is due in part to the retrograde spin geometry of IC 694.

4. The tidal morphology is unique among mergers: there is a low surface brightness stellar tail with low column density H I and a conspicuous parallel gaseous tail of higher H I column density and with little, if any, associated starlight. The tails have very similar kinematics, suggesting that they are physically connected. We suggest that such bifurcated or parallel tails result from a progenitor with a

[13] Using a velocity dispersion of 20 km s^{-1} as inferred for the stars in § 3.2 would give $M_{\rm lum}/M_{\rm dyn} < 0.04$ on this feature.

warped disk. However, this explanation does not explain the low H I content of the optical tail.

5. The similarity between this tidal morphology and that of other starburst galaxies with direct evidence of superwind outflows (M82, NGC 4631, NGC 520, Arp 220) suggest that the galactic superwind recently imaged by Heckman et al. (1999) may be responsible for clearing the optical tail of much of its cold diffuse gas. Local ionizing sources within the tidal tails may also play a role in some of the observed optical/gaseous anticorrelation. These issues are explored in more detail in HVY99

6. The absence of dwarf-galaxy–like mass concentrations in the tidal tail suggests that tidal dwarf formation is not a ubiquitous process. It is possible that whatever process removed the gas from the optical tail may have consequently suppressed the dwarf formation process.

We would like to thank S. Aalto, L. Armus, F. Casoli, and F. Combes for sharing data and information prior to publication. We thank the referee, Tim Heckman, for a timely and useful report that helped clarify many areas of this paper. J. E. H. would like to thank the Owens Valley group at Caltech, and in particular Nick Scoville, for the hospitality extended during the summer of 1995 to reduce the H I data presented in this paper. Thanks also to W. Vacca, J. van Gorkom, J. Barnes, and G. Stinson for useful conversations. J. E. H. acknowledges support by grant HF-1059.01-94A from the Space Telescope Science Institute, which is operated by the Association of Universities for Research in Astronomy, Inc., under NASA contract NAS 5-26555, for much of this research. Most of the figures in this paper were made with the WIP interactive software package (Morgan 1995). This research has made extensive use of the NASA/IPAC Extragalactic Database (NED), which is operated by the Jet Propulsion Laboratory, California Institute of Technology, under contract with the National Aeronautics and Space Administration. The Digitized Sky Surveys were produced at the Space Telescope Science Institute under U.S. Government grant NAG W-2166. The images of these surveys are based on photographic data obtained using the Oschin Schmidt Telescope on Palomar Mountain and the UK Schmidt Telescope. The plates were processed into the present compressed digital form with the permission of these institutions.

APPENDIX

WHICH GALAXY IS IC 694?

There is some confusion in the printed and electronic literature as to which systems actually comprise Arp 299 (e.g., Yamaoka et al. 1998; NED).[14] Arp does not offer many clues and even confuses the matter by incorrectly designating Arp 296 as NGC 3690 + IC 694 in Tables 1 and 2 of his Atlas, while giving Arp 299 no further designation (Arp 1966). However, the description in Arp's Table 1 and the order of his figures (with Arp 296 appearing next to other bridge-tail systems) makes it clear that Arp published the pictures under the correct number and gave them the correct description in Table 1, but simply got the "designation" switched in both tables.

The description given for NGC 3690 in the NGC (Dreyer 1888) translates as "pretty bright, pretty small, very little extended at P.A. = 80, pretty gradually brighter toward the middle, small stars south following near." According to the NGC, "pretty small" means a diameter of 50″–60″, and this radius would incorporate much of the brighter parts of the system (including the nucleus of the eastern system). Given that the five highest surface brightness objects are within 7″ of source B in the western system, through a small telescope this object must have looked like a single nucleus at the location of source B in Figure 1 with a cloud of surrounding nebulosity, and it is unlikely that two nuclei could have been discerned. It therefore seems likely that the original designation refers to the entire Arp 299 system, although only one nucleus was identified (corresponding to the western system, what we have been calling NGC 3690 here). Therefore whether NGC 3690 should strictly apply to the entire system or to only the western system depends on whether one believes that galaxies are identified by their nuclei or their integrated light. We remain agnostic on this point, and from here investigate which object was designated as IC 694.

The earliest and clearest association of IC 694 with the eastern system can be traced to Vorontsov-Velyaminov in his Atlas and Catalogue of Interacting Galaxies (Vorontsov-Velyaminov 1959), where Arp 299 appears as VV118a-e. Source VV118a is the galaxy to the east (what we have been referring to as IC 694), VV118b the system to the west (what we have been calling NGC 3690); VV118c is MCG + 10-17-2a, the compact spheroidal 1′ to the northwest, and VV118d & e are bright H II regions in the outer disk to the northwest. In the accompanying table to the Atlas, VV118a is identified as IC 694, VV118b as NGC 3690, and sources c, d, and e have no other designations. The vast majority of researchers since have followed this designation. Nilson first brings up the question of the identification of IC 694 with VV 118a in the UGC (Nilson 1973) in his notes on UGC 6471/2: "Arp 296 (identified as NGC 3690 + IC 694 by Arp) are faint objects north-preceding UGC 06471 + UGC 06472, magnitude approximately 17 and 21 identification of IC 694 uncertain, may be a small object north-preceding and inside the outer parts of the double system." (The use of the name Arp 296 is immediately attributed to Arp's error in making his tables, as discussed above).

IC 694 was discovered by Swift (1893), whose discovery description translates as "close double with NGC 3690 = object 247 of list I of Sir William Herschel. Suspected at 132 × magnification, verified at 200 ×." In the Index Catalogue of Nebulae (IC; Dreyer 1895) this becomes "very small, forms double nebula with no. 247 of list I of Sir William Herschel." "Very small"

[14] For this discussion it is instructive to look at an earlier photographic representation of the Arp 299. For this, we refer to reader to Plate 1 of Morgan (1958). In this figure, the northwest spheroidal appears as a very faint fuzz well separated from and much dimmer than either of the two interacting disks, which appear as distinct objects.

translates as 10″–20″ in diameter, which is on the large side for the northwest spheroidal ($\theta_{\rm FWHM} \sim 4''$). There is no definition of the term "double" in the IC,[15] and perhaps this is where the confusion lies. Certainly, with today's knowledge we would call Arp 299E + W a double, and the spheroidal to the northwest, a possible companion. However, is this how Dreyer and Swift used the term?

So the question is, when Swift identified IC 694, did he subdivide the NGC 3690 entry or add an entry for the faint nebulosity to the northwest? The position for IC 694 is given as 11:20:44 +59:20 (epoch 1860) in the IC, while the NGC position for NGC 3690 is 11:20:45 +59:19; i.e., IC 694 lies approximately 1′ to the northwest of NGC 3690. This seems to be pretty conclusive evidence that IC 694 indeed refers to the spheroidal to the northwest. However, Dreyer remarks in the introduction to the IC that Swift's positions are "generally reliable within one or two minutes of arc, but larger errors occur occasionally."

We also learn from Dreyer that Swift's observations were taken through a 16″ refractor at the Rochester Observatory. Since the northwest galaxy is 3 mag fainter than either of the disk galaxies ($m_B = 16.2$ mag from CCD observations reported above), is it even possible for Swift to have seen the northwest companion? If not, it is likely that he simply resolved NGC 3690 into two separate condensations of nearly equal luminosity, adding a separate catalogue entry for the second system. A similar super-classification appears to have happened in the case of NGC 4861/IC 3961 (Arp 266) and NGC 2207/IC 2163.

Recent attempts to repeat these observations with similar-sized telescopes by amateur astronomers suggest that (1) the second light concentration now associate with the nucleus of Arp 299E is very easy to discern as distinct from Arp 299W and (2) the northwest spheroidal is indeed a *very* difficult, but not impossible, object. Combined with the correct relative position of IC 694 given by Swift, it seems that there is strong evidence that IC 694 properly designates the northwest compact spheroidal. However, since these observations were made with prior knowledge of both the existence and location of the northwest spheroidal, this confirmation is not entirely independent. Since it is nearly impossible to resolve this issue conclusively one way or the other, we choose to follow the vast majority of researchers and use the designation introduced by Vorontsov-Velyaminov (1959), concluding with Sulentic & Tift (1973) that "any further question as to which objects Dreyer was referring to can only be of historical interest."

J. E. H. offers special thanks to Harold Corwin, Steve Gottleib, Malcom Thomson, Bill Vacca, and Dennis Webb for many useful discussions on this issue.

REFERENCES

Aalto, S., Radford, S. J. E., Scoville, N. Z., & Sargent, A. I. 1997, ApJ, 475, L107
Aaronson, M. Huchra, J., Mould, J., Schechter, P. L., & Tully, R. B. 1982, ApJ, 258, 64
Alton, P. B., Trewhella, M., Davies, J. I., Evans, R., Bianchi, S., Gear, W., Thronson, H., Valentijn, E., & Witt, A. 1998, A&A, 335, 807
Anantharamaiah, K. R., Zhao, J.-H., Goss, W. M., & Viallefond, F. 1993, ApJ, 419, 585
Appleton, P. N., Ghigo, F. D., van Gorkom, J. H., Schombert, J. M., & Struck-Marcell, C. 1987, Nature, 330, 140
Armus, L., Heckman, T. M., & Miley, G. K. 1989, ApJ, 347, 727
———. 1990, ApJ, 364, 471
Arp, H. C. 1966, ApJS, 14, 1
Augarde, R., & Lequeux, J. 1985, A&A, 147, 273
Baan, W. A. 1985, Nature, 315, 26
Baan, W. A., & Haschick, A. 1990, ApJ, 364, 65 (BH90)
Barnes, J. E. 1988, ApJ, 331, 699
———. 1992, ApJ, 393, 484
Barnes, J. E., & Hernquist, L. 1992, Nature, 360, 715
———. 1996, ApJ, 471, 115
Beck, S. C., Turner, J. L., & Ho, P. T. P. 1990, ApJ, 349, 57
Binney, J., & Tremaine S. 1987, Galactic Dynamics (Princeton: Princeton Univ. Press)
Bosma, A. 1981, AJ, 86, 1791
———. 1991, in Warped Disks and Inclined Rings around Galaxies, ed. S. Casertano, P. Sackett, & F. Briggs (Cambridge: Cambridge Univ. Press), 181
Bottema, R. 1993, A&A, 275, 16
Bregman, J. N., Hogg, D. E., & Roberts, M. S. 1992, ApJ, 387, 484
Briggs, D.S. 1995, Ph.D. thesis, New Mexico Inst. Mining & Technology
Broeils, A. H., & van Woerden, H. 1994, A&AS, 107, 129
Bushouse, H. A., & Gallagher, J. S., III. 1984, PASP, 96, 273
Carico, D. P., Sanders, D. B., Soifer, B. T., Matthews, K., & Neugebauer, G. 1990, AJ, 100, 70
Carral, P., Turner, J. L., & Ho, P. T. P. 1990, ApJ, 362, 434
Casoli, F., Combes, F., Augarde, R., Fign, P., & Martin, J. M. 1989, A&A, 224, 31
Casoli, F., Willaime, M.-C., Viallefond, F., & Gerin, M. 1999, A&A, 346, 663
Cayatte, V., van Gorkom, J. H., Balkowski, C., & Kotanyi, C. 1994, AJ, 107, 1003
Chevalier, R. A., & Clegg A. W. 1985, Nature, 317, 44
Condon, J. J., Condon, M. A., Gisler, G., & Puschell, J. J. 1982, ApJ, 252, 102
Condon, J. J., Helou, G., Sanders, D. B., & Soifer, B. T. 1990, ApJS, 73, 359
Condon, J. J., Huang, Z.-P., Yin, Q. F., & Thuan, T. X. 1991, ApJ, 378, 65
Dahlem, M., Heckman, T. M., Fabbiano, G., Lehnert, M. D., & Gilmore, D. 1996, ApJ, 461, 724
de Blok, W. J. G., & van der Hulst, J. M. 1998, A&A, 336, 49
de Jong, R. S. 1995, Ph.D. thesis, Univ. Groningen
Dickey, J. M. 1982, ApJ, 263, 87
Dickey, J. M., Brinks, E., & Puche, D. 1992, ApJ, 385, 501
Doherty, R. M., Puxley, P. J., Lumsden, S. L., & Doyon, R. 1995, MNRAS, 277, 577
Donahue, M., Aldering, G., & Stocke, J. T. 1995, ApJ, 450, L45
Dreyer, J. L. E. 1888, MmRAS, 49, 1
———. 1895, MmRAS, 51, 185
Duc, P.-A., Brinks, E., Wink, J. E., & Mirabel, I. F. 1997, A&A, 326, 537
Dudley, C. C. 1998, Ph.D. thesis, Univ. Hawaii
Dudley, C. C., & Wynn-Williams, C. G. 1993, ApJ, 407, L65
Elmegreen, B., Kaufmann, M., & Thomasson, M. 1993, ApJ, 412, 90
Fairall, A. P. 1971, MNRAS, 153, 303
Gehrz, R. D., Sramek, R. A., & Weedman, D. W. 1983, ApJ, 267, 551
Giovanelli, R., & Haynes, M. P. 1990, in Galactic and Extragalactic Radio Astronomy, ed. G. L. Verschuur, K. I. Kellermann (New York: Springer), 522
Gooch, R. E. 1995, in ASP Conf. Series, 101, Astronomical Data Analysis Software and Systems V, ed. G. H. Jacoby & J. Barnes (San Francisco: ASP), 80
Heckman, T. M., Armus, L., & Miley, G. K. 1990, ApJS, 74, 833
Heckman, T. M., Armus, L., Weaver, K. A., & Wang, J. 1999, ApJ, 517, 130
Heckman, T. M., Lehnert, M., & Armus, L. 1993, in The Evolution of Galaxies and their Environment, ed. H. A. Thronson and J. M. Shull (Dordrecht: Kluwer), 455
Hibbard, J. E. 1995, Ph.D. thesis, Columbia Univ.
Hibbard, J. E., Bland-Hawthorn, J., Tully, R. B. 1999a, in preparation
Hibbard, J. E., Guhathakurta, P., van Gorkom, J. H., & Schweizer, F. 1994, AJ, 107, 67
Hibbard, J. E., & Mihos, J. C. 1995, AJ, 110, 140
Hibbard, J. E., Vacca, W. D., & Yun, M. S. 1999b, AJ, submitted (HVY99)
Hibbard, van der Hulst, & Barnes 1999c, in preparation
Hibbard, J. E., & van Gorkom, J. H. 1993, in ASP Conf. Series, 48, The Globular Cluster-Galaxy Connection, ed. G. H. Smith & J. P. Brodie (San Francisco: ASP), 619
———. 1996, AJ, 111, 655 (HvG96)
Hibbard, J. E., & Yun, M. S., 1996, in Cold Gas at High Redshift, ed. M. Bremer, H. Rottgering, P. van der Werf, & C. L. Carilli (Dordrecht: Kluwer), 47

[15] Ironically, in the introduction to the IC Dreyer states "the system of abbreviated description...has been in use so long that it is unnecessary to enter into a lengthy explanation of it."

Hibbard, J. E., & Yun, M. S. 1999, in preparation
Hilker, M., & Kissler-Patig, M. 1996, A&A, 314, 357
Hoffman, L. G., Salpeter, E. E., Farhat, B., Roos, T., Williams, H., & Helou, G. 1996, ApJS, 105, 269
Hogg, D. E., Roberts, M. S., & Sandage, A. 1993, AJ, 106, 907
Huchtmeier, W. K., & Richter, O. -G. 1988, A&A, 203, 237
Hunsberger, S., Charlton, J., & Zaritsky, D. 1996, ApJ, 462, 50
Hutchings, J. B. 1996, AJ, 111, 712
Jones, T. J., 1997, AJ, 114, 1393
Jones, T. J., Gehrz, R. D., & Smith, J. 1990, AJ, 99, 1470
Joy, M., Lester, D. F., Harvey, P. M., Telesco, C. M., Decher, R., Rickard, L. J., & Bushouse, H. 1989, ApJ, 339, 100
Kalberla, P. M. W., Schwarz, U. J., & Goss, W. M. 1985, A&A, 144, 27
Kaufman, M., Brinks, E., Elmegreen, D. M., Thomasson, M., Elmegreen, B. G., Struck, C., & Klaric, M. 1997, AJ, 114, 2323
Keel, W. C., Kennicutt, R. C., Jr., Hummel, E., & van der Hulst, J. M. 1985, AJ, 90, 708
Kennicutt, R.B., Jr. 1998, ApJ, 498, 541
Kinney, A. L., Bohlin, R. C., Calzetti, D., Panagia, N., Wyse, R. F. G. 1993, ApJS, 86, 5
Kobulnicky, H. A., & Dickey, J. M. 1999, AJ, 117, 908
Lançon, A., Rocca-Volmerang, B., & Thuan, T. X. 1996, A&AS, 115, 253
Landolt, A. U. 1983, AJ, 88, 439
Lees, J. F., Knapp, G. R., Rupen, M. P., & Phillips, T. G. 1991, ApJ, 379, 117
Lehnert, M. D., & Heckman, T. M. 1996, ApJ, 462, 651
Malphrus, B. K., Simpson, C. E., Gottesman, S. T., & Hawarden, T. G. 1997, AJ, 114, 1427
Mazzarella, J. M., & Boroson, T. A. 1993, ApJS, 85, 27
Meurer, G. R., Heckman, T. M., Leitherer, C., Kinney, A., Robert, C., & Garnett, D. R. 1995, AJ, 110, 2665
Mihos, J. C., & Bothun, G. D. 1998, ApJ, 500, 619
Mihos, J. C., & Hernquist, L. 1994, ApJ, 437, L47
———. 1996, ApJ, 464, 641
Miles, J. W., Houck, J. R., Hayward, T. L., & Ashby, M. L. N. 1996, ApJ, 465, 191
Mirabel, I. F., Dottori, H., & Lutz, D. 1992, A&A, 256, L19
Morgan, J. A. 1995, in ASP Conf. Ser. 77, Astronomical Data Analysis Software and Systems IV, ed. R. A. Shaw, H. E. Payne, & J. J. E. Hayes (San Francisco: ASP), 129
Morgan, W. W. 1958, PASP, 70, 364
Murphy, T. W., Jr., Armus, L., Matthews, K., Soifer, B. T., Mazzarella, J. M., Shupe, D. L., Strauss, M. A., & Neugebauer, G. 1996, AJ, 111, 1025
Nakagawa, T. N., Nagata, T., Geballe, T. R., Okuda, H., Shibai, H., & Matsuhara, H. 1989, ApJ, 340, 729
Nilson, P. 1973, Uppsala General Catalogue of Galaxies (Stockholm: Almqvist & Wiksell)
Noguchi, M. 1991, MNRAS, 251, 360
Nordgren, T. E., Chengalur, J. N., Salpeter, E. E., & Terzian, Y. 1997, AJ, 114, 77
Olson, K. M., & Kwan, J. 1990, ApJ, 361, 426
Ridgeway, S. E., Wynn-Williams, C. G., & Becklin, E. E. 1994, ApJ, 428, 609
Rieke, G. H. 1988, ApJ, 331, L5
Roberts, C. 1996, in Proc. of the 11th IAP Astrophysics Meeting, The Interplay Between Massive Star Formation, the ISM, and Galaxy Evolution, ed. D. Kunth, B. Guiderdoni, M. Heydari-Malayeri, & T. X. Thuan, (Gif-sur-Yvette: Ed. Frontières), 371
Roberts, M. S., & Haynes, M. P. 1994, ARA&A, 32, 115
Rupen, M. P. 1999, in ASP Conf. Ser., Aperture Synthesis in Radio Astronomy, ed. G. B. Taylor, C. L. Carilli, & R. A. Perley (San Francisco: ASP) in press
Sanders, D. B., Scoville, N. Z., & Soifer, B. T. 1991, ApJ, 370, 158
Sanders, D. B., Soifer, B. T., Elias, J. H., Madore, B. F., Matthews, K., Neugebauer, G., & Scoville, N. Z. 1988, ApJ, 325, 74
Sargent, A. I., & Scoville, N. Z. 1991, ApJ, 366, L1
Sargent, W. L. W. 1972, ApJ, 173, 7
Schombert, J. M., Wallin, J. F., & Struck-Marcell, C. 1990, AJ, 99, 497
Schweizer, F. 1978, in IAU Symp. 77, The Structure and Properties of Nearby Galaxies, ed. E. M. Berkhuijsen & R. Wielebinski (Dordrecht: Reidel), 279
Scoville, N. Z., Hibbard, J. E., Yun, M. S., & van Gorkom, J. H. 1994, Mass-Transfer Induced Activity in Galaxies, ed. I. Shlosman (Cambridge: Cambridge Univ. Press), 191
Shier, L. M., Rieke, M. J., & Rieke, G. H. 1996, ApJ, 470, 222
Silva, D. R., & Bothun, G. D. 1998, AJ, 116, 85
Smith, B. J., Struck, C., & Pogge, R. W. 1997, ApJ, 483, 754
Smith, B. J. 1994, AJ, 107, 1695
Smith, D. A., Herter, T., Haynes, M. P., Beichman, C. A., & Gautier, T. N. 1996, ApJS, 104, 217
Smith, H. E., Lonsdale, C. J., & Lonsdale, C. J. 1998, ApJ, 492, 137
Solomon, P. M., Downes, D., Radford, S. J. E., & Barrett, J. W. 1997, ApJ, 478, 144
Stanford, S. A. 1989, Ap&SS, 157, 117
Stanford, S. A., & Wood, D. O. S. 1989, ApJ, 346, 712
Sulentic, J. W., & Tift, W. G. 1973, The Revised New General Catalogue of Nonstellar Astronmical Objects (Tucson: Univ. Arizona Press)
Swift, L., 1893, MNRAS, 53, 273
Taff, L. G., Lattanzi, M. G., Bucciarelli, B., Gilmozzi, R., McLean, B. J., Jenkner, H., Laidler, V. G., Lasker, B. M., Shara, M. M., & Sturch, C. R. 1990, ApJ, 353, L45
Taniguchi, Y., & Ohyama, Y. 1998, ApJ, 509, L89
Telesco, C. M., Decher, R., & Gatley, I. 1985, ApJ, 299, 896
Toomre, A., & Toomre, J. 1972, ApJ, 178, 623 (TT72)
Tully, R. B. 1988, Nearby Galaxy Catalog (Cambridge: Cambridge Univ. Press)
Vacca, et al. 1999
van der Hulst, J. M. 1979, A&A, 155, 151
van der Kruit, P. C. 1988, A&A, 192, 117
van Driel, W., & van Woerden, H. 1991, A&A, 243, 71
van Zee, L., Haynes, M. P., & Salzer, J. J. 1997, AJ, 114, 2497
Vorontsov-Velyaminov, B. A. 1959, Atlas and Catalogue of Interacting Galaxies (Moscow: Sternberg Inst.)
Wang, B. 1995, ApJ, 444, 590
Wardle, M., & Knapp, G. R. 1986, AJ, 91, 23
Weliachew, L., Sancisi, R., & Guelin, M. 1978, A&A, 65, 37
Wevers, B. H. M. R., Appleton, P. N., Davies, R. D., & Hart, L. 1984, A&A, 140, 125
Wevers, B. H. M. R., van der Kruit, P. C., & Allen, R. J. 1986, A&AS, 66, 505
White, S. D. M. 1979, MNRAS, 189, 831
Witt, A. N., Thronson, H. A., & Capuano, J. M., Jr. 1992, ApJ, 393, 611
Wynn-Williams, C. G., Eales, S. A., Becklin, E. E., Hodapp, K.-W., Joseph, R. D., McLean, I. S., Simons, D. A., & Wright, G. S. 1991, ApJ, 377, 426
Yamaoka, H., Kato, T., Filippenko, A. V., & Van Dyk, S. D. 1998, IAU Circ. 6859
Young, J. S., & Knezek, P. M. 1989, ApJ, 347, L55
Young, J. S., & Scoville, N. Z. 1991, ARAA, 29, 581
Yun, M. S., & Hibbard, J. E. 1999, APJ, submitted
Yun, M. S., Hibbard, J. E., & Scoville, N. Z. 1999, in preparation
Yun, M. S., Ho, P. T. P., & Lo, K. Y. 1993, ApJ, 411, L17
———. 1994, Nature, 372, 530
Zezas, A. L., Georgantopoulos, I., & Ward, M. J. 1998, MNRAS, 301, 915
Zhao, J.-H., Anantharamaiah, K. R., Goss, W. M., & Viallefond, F. 1997, ApJ, 482, 186